ARL-TR-8860 ● Nov 2019

Dynamic Compression Strength of Ceramics: Results from an Interlaboratory Round-Robin Exercise

by Jeffrey J Swab and George D Quinn

NOTICES

Disclaimers

The findings in this report are not to be construed as an official Department of the Army position unless so designated by other authorized documents.

Citation of manufacturer's or trade names does not constitute an official endorsement or approval of the use thereof.

Destroy this report when it is no longer needed. Do not return it to the originator.

ARL-TR-8860 ● Nov 2019

Dynamic Compression Strength of Ceramics: Results from an Interlaboratory Round-Robin Exercise

Jeffrey J Swab
Weapons and Materials Research Directorate, CCDC Army Research Laboratory

George D Quinn
National Institute of Standards and Technology

REPORT DOCUMENTATION PAGE

Form Approved
OMB No. 0704-0188

1. REPORT DATE *(DD-MM-YYYY)*	2. REPORT TYPE	3. DATES COVERED (From - To)
November 2019	Technical Report	1 November 2017–30 April 2019

4. TITLE AND SUBTITLE
Dynamic Compression Strength of Ceramics: Results from an Interlaboratory Round-Robin Exercise

5a. CONTRACT NUMBER

5b. GRANT NUMBER

5c. PROGRAM ELEMENT NUMBER

6. AUTHOR(S)
Jeffrey J Swab and George D Quinn

5d. PROJECT NUMBER

5e. TASK NUMBER

5f. WORK UNIT NUMBER

7. PERFORMING ORGANIZATION NAME(S) AND ADDRESS(ES)
CCDC Army Research Laboratory
ATTN: FCDD-RLW-ME
Aberdeen Proving Ground, MD 21005

8. PERFORMING ORGANIZATION REPORT NUMBER
ARL-TR-8860

9. SPONSORING/MONITORING AGENCY NAME(S) AND ADDRESS(ES)

10. SPONSOR/MONITOR'S ACRONYM(S)

11. SPONSOR/MONITOR'S REPORT NUMBER(S)

12. DISTRIBUTION/AVAILABILITY STATEMENT
Approved for public release; distribution is unlimited.

13. SUPPLEMENTARY NOTES
ORCID ID(s): Jeffrey Swab, 0000-0002-8204-7202

14. ABSTRACT

The dynamic compressive strength of a commercial alumina was determined by five participants using the split-Hopkinson pressure bar (SHPB) method with a dumbbell-shaped specimen. Each participant used their own SHPB test apparatus and imaging setup to conduct the tests and capture the fracture process. The dumbbell-shaped specimen was designed to increase the likelihood of fracture commencing in the specimen gage section rather than at the interface of the specimen and the SHPB bars. The participants had a good success rate (between 40% and 80%) of tests being valid, even though this was the first time several of the participants had used this specimen geometry. The average dynamic compression strength from the five participants was in excellent agreement with each other and ranged from 4.40 to 4.92 GPa with a grand average of 4.61 ± 0.25 GPa (the average of the laboratory averages). The high success rate and remarkable consistency of the results show that the dumbbell-shaped specimen is an appropriate geometry to determine the dynamic compression strength of advanced ceramics using the SHPB test methodology.

15. SUBJECT TERMS
dynamic compression strength, split-Hopkinson pressure bar (SHPB), round robin, alumina, ceramics

16. SECURITY CLASSIFICATION OF:			17. LIMITATION OF ABSTRACT	18. NUMBER OF PAGES	19a. NAME OF RESPONSIBLE PERSON
a. REPORT	b. ABSTRACT	c. THIS PAGE			Jeffrey Swab
Unclassified	Unclassified	Unclassified	UU	58	19b. TELEPHONE NUMBER (Include area code) (410) 306-0753

Standard Form 298 (Rev. 8/98)
Prescribed by ANSI Std. Z39.18

Contents

List of Figures

List of Tables

Acknowledgments

The authors would like to acknowledge the following participants for the time and energy spent testing and analyzing the data as well as answering the authors' repeated questions. Their attention to detail was greatly appreciated.

- Dr Christopher Meredith and Dr John J Pittari III of the CCDC Army Research Laboratory (ARL)
- Dr Steve Mates of the National Institute of Standards and Technology (NIST)
- Dr Richard Rhorer of Rhorer Precision Engineering, who assisted Dr Mates
- Dr Wayne Chen and Dr Hangjie Liao of Purdue University
- Dr James Hogan and Mr Calvin Lo at the University of Alberta

The views and conclusions contained in this report are those of ARL and NIST. Citation of manufacturer's or trade names for specific test equipment, materials, software, or test methodologies does not constitute an official endorsement or approval of the use thereof.

1. Introduction

Advanced ceramics such as boron carbide, silicon carbide, and alumina are being used, or considered for use, in a variety of systems designed to protect vehicles and individuals against high-energy impact events. The impact events of interest typically create a peak strain rate of 10^4/s to 10^6/s on the ceramic.[1–3] Test methodologies used to evaluate and predict the performance of ceramics at these strain rates are limited in number, cumbersome, time-consuming, and expensive. Additionally, the methods are not conducive to material development and screening as each requires a substantially large ceramic specimen.

On the other hand, there is a plethora of standardized methods for evaluating the strength, fracture toughness, hardness, and other properties of ceramics at quasi-static strain rates (10^{-3} to 10^0/s). These methods, when compared to the high-rate test methods, are quick, simple, inexpensive, and applicable to material development and screening as they require significantly smaller test specimens. Unfortunately, there is minimal evidence directly linking any of these properties, or a combination of properties and failure mechanisms, to the performance of the ceramic during a high-strain-rate impact event.

The split-Hopkinson pressure bar (SHPB) method may help bridge this information gap as strain rates between 10^2/s and 10^5/s can be reached in materials that plastically deform. Unfortunately, ceramics are brittle and have a maximum strain at fracture around 1% in compression. The strain at fracture in tension is much lower. To ensure that force equilibrium exists in a ceramic specimen when compression fracture occurs and the strain rate has stabilized during the loading ramp, the strain rate should be less than 3000/s.[4,5] The SHPB method is applicable to materials development and screening since the volume of material needed is similar to what is used in many quasi-static tests. The dynamic compression strength,[6–16] flexure strength,[17] and hardness[18,19] of advanced ceramics have been determined, in this strain rate regime, using test methods based on the SHPB methodology.

This interlaboratory round-robin exercise was organized and conducted between 2018 and 2019 to examine the dynamic compression strength of ceramics using the SHPB method. It was motivated by two factors. The first was to deal with unresolved issues that were identified at a workshop held in 2005 on testing ceramics using the SHPB method.[20] At the workshop many SHPB experts discussed the nuances of SHPB testing procedures, such as whether high-speed imaging was necessary to document the fracture process, the value of the ceramic compression strength data, the validity and consistency of this data, and the merits and drawbacks associated with the myriad of specimen geometries and dimensions

that have been used. The discussions were valuable, but no consensus was reached on any topic and a proposed round robin using both dumbbell and cylindrical shaped alumina specimens was greeted with mixed responses.*

Even today, the varied specimen geometries are of special concern. Typically, a cuboidal or cylindrical specimen is used in the SHPB test. This is appropriate for testing metals that exhibit plastic deformation during loading but not for ceramics, which are brittle with very low fracture strain in compression. In many instances when ceramic cuboids or cylinders are used, fracture results from an axial crack or cracks that initiate at the specimen/bar interface and propagate parallel to the loading direction. This is a clear indication that a *lateral* tensile stress is dominant and *not* an axial compressive stress. A dumbbell-shaped specimen as shown in Fig. 1 was designed in the 1980s and used to measure the quasi-static compression strength of ceramics.[21–23] There were precedents for this specimen geometry as earlier work by Sines and Adams,[24] Birch et al.,[25] and Bortz and Burton[26] had used dumbbell compression specimens. Dumbbell-shaped specimens have also been successfully used to determine the dynamic compression strength of ceramics using the SHPB method.[27–31] Additionally, dynamic simulations have determined that the dumbbell shape is the best specimen geometry for testing ceramics using the SHPB method.[32]

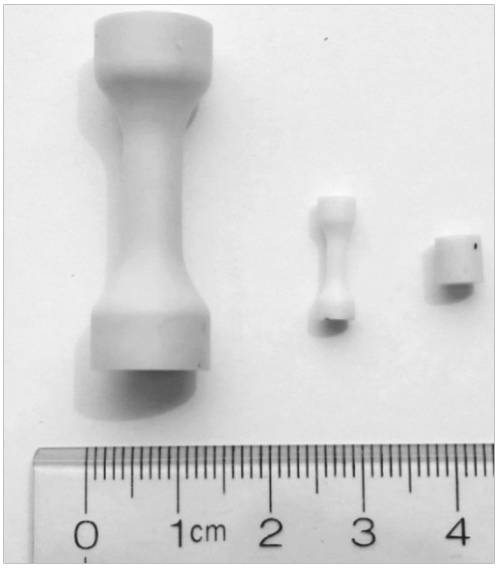

Fig. 1 Ceramic compression strength specimens. Left: Full-sized Coors AD-94 dumbbell specimen as used by Tracy[21] for static strength determination in 1987. This size was later labeled the "A" size by Dunlay et al.[22] Middle: CoorsTek CERASHIELD CAP3 specimen used in the round robin described in this report. Right: Typical-sized AD999 specimen of the type commonly used for static or dynamic compression strength testing.

* Many representatives from industry, ceramic manufacturers, government, and a few SHPB laboratories were enthusiastic about conducting a multifaceted round robin, but some SHPB testing laboratories were reluctant.

The second motivation for conducting this exercise was to address a prevailing problem in the literature about poor data consistency. Published ceramic compression strength values can vary by as much as a factor of 2. So, for example, dumbbell-shaped specimens yielded a quasi-static compression strength of 6.1 ± 0.3 GPa and a dynamic strength of 6.2 ± 0.3 GPa (10^2/s) for a hot-pressed boron carbide.[31] A previous effort[27,28] reported a similar strength for the same hot-pressed boron carbide using a smaller dumbbell-shaped specimen. Both of these quasi-static values obtained with the dumbbell-shaped specimens were almost 50% higher than the value listed on the supplier's website that was obtained with a right cylinder following the guidelines in ASTM C773*. Others[33–36] have used cuboids of different sizes and reported quasi-static values from 1 to 4 GPa and values from SHPB tests between 2 and 5.7 GPa for hot-pressed boron carbide.

The purpose of the round robin was to answer the following questions:

1) Is the dumbbell shape the appropriate specimen geometry for testing high-strength ceramics using the SHPB method?

2) Can consistent compression strength values be obtained using the dumbbell specimen?

3) Are there any potential issues related to the testing of these specimens in the SHPB?

2. Material

The material chosen for this exercise was a sintered 99.5% pure alumina from CoorsTek labeled as CERASHIELD CAP3†. The general properties of this material are summarized in Table 1 and images of the microstructure are provided in Fig. 2. It should be noted that the CAP3 alumina is different from the AD995 alumina that is also produced by CoorsTek. While both materials have the exact same composition and general properties, per the CoorsTek website, it has been reported that the AD995 version has a finer grain size than the CAP3.[37]

* ASTM C773. *Standard Test Method for Compressive (Crushing) Strength of Fired Whiteware Materials*. West Conshohocken (PA): ASTM International.
† CoorsTek, Golden, CO, USA.

Table 1 General properties of the CoorsTek CERASHIELD CAP3 alumina[*]

Property	Method	Value
Density (g/cm^3)	ASTM C20	3.90
Flexure strength (MPa)	ASTM F417	379
Elastic modulus (GPa)	ASTM C848	370
Compressive strength (GPa)	ASTM C773	2.5
Hardness (GPa)	Knoop 1000 gf	14.1
Fracture toughness (MPa√m)	Notched Beam[a]	4.0–5.0

[a] The notched beam method is not a standardized method for determining the fracture toughness of ceramics as it overestimates the value.[†]

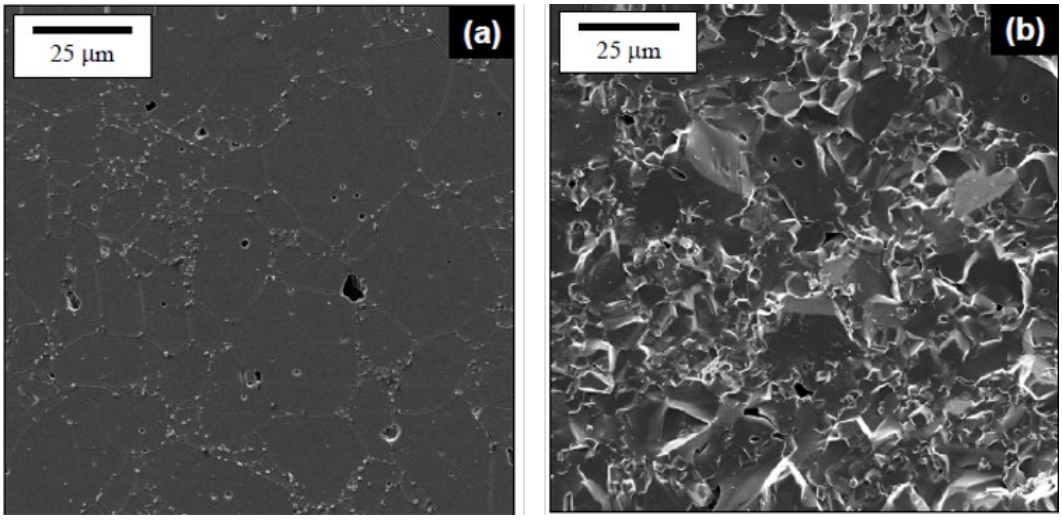

Fig. 2 Microstructure of CoorsTek CERASHIELD CAP3 alumina: a) polished surface, b) fracture surface

Small dumbbell-shaped specimens with the dimensions shown in Fig. 3 were machined from a single 1-inch-thick plate of the CAP3 material. This specimen is a scaled-down version of the dumbbell specimen developed by Tracy et al.[21–23] and is similar to the specimen used by Blumenthal et al.[27,28] Figure 1 shows the comparative sizes of the older "A" specimen[22] and the new miniature dumbbell specimen used in this exercise. The miniaturization is beneficial for several reasons. First, while the larger specimen can be tested to failure in quasi-static loading relatively easily using a universal test frame with a very large load capacity, it may be difficult, if not impossible, to generate the large stresses necessary to fracture

[*] https://www.coorstek.com/media/2764/ceramic-armor-overview.pdf.

[†] ASTM C1421. *Standard Test Methods for Determination of Fracture Toughness of Advanced Ceramics at Ambient Temperature.* West Conshohocken (PA): ASTM International. ASTM Book of Standards, Vol. 15.01; 2018.

the specimen in many SHPB apparatuses. Second, it is easier to reach stress equilibrium under SHPB loading with smaller specimens. Finally, the smaller specimen is more versatile. It allows for more specimens to be machined from a single ceramic plate—an important consideration when dealing with material uniformity issues in a round-robin exercise—and it enables specimens to be machined at different orientations relative to a plate dimension, providing the opportunity to determine if strength anisotropy exists.

All specimens were machined with the long axis parallel to the plate thickness, using conventional diamond tooling to a final 320-grit surface finish. Every single specimen was examined with an optical comparator to ensure the dimensions and associated tolerances were within the specifications in Fig. 3. Every specimen was also optically examined with a stereo-optical microscope for surface damage such as chips and extraneous machining damage that may influence the fracture process. All the specimens used in this exercise met the dimensional specifications, and the surfaces were free of chips and extraneous machining damage.

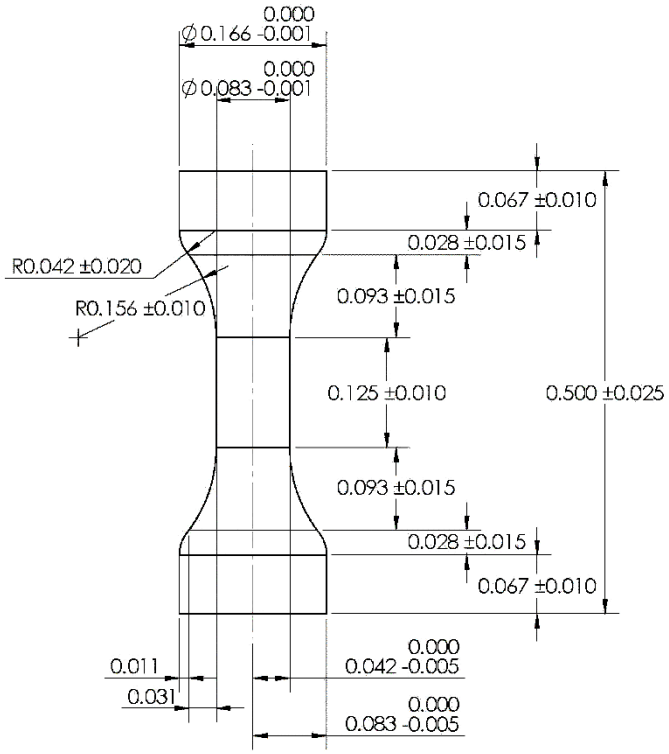

Fig. 3 The dumbbell-shaped specimen tested in this exercise. All dimensions are in inches.

3. Instructions

The five participating organizations in this exercise were from Purdue University, the National Institute of Standards and Technology, the University of Alberta, and two separate participants in two different groups from the Army Research Laboratory. Each participant was provided 10 dumbbell specimens with instructions to determine the dynamic compression strength using the SHPB method. The target was to obtain three to five (preferably five) valid test results from each participant. Extra specimens were provided to allow participants to practice using these specimens on their SHPB apparatus or to make up for unsuccessful or invalid outcomes. The participants were also asked to determine the strain rate for each specimen tested and use a high-speed imaging system to capture the fracture process.

In addition, the participants were required to provide the information outlined in Appendix A and below on their SHPB apparatus, high-speed imaging system, and information on each tested specimen. They were also asked how much experience they had testing ceramics by SHPB. We asked about these topics since there are many variables and nuances of testing that could affect the outcome of the round robin. Many of these variations had been identified in the earlier 2005 workshop.[20] The participants were asked to provide details about the following:

- **SHPB setup**: The striker, incident, and transmission bar materials, and diameter and length of each bar; a picture of their SHPB setup; a brief description of the unit and the testing procedures; the strain rate measurement method used; the striker bar velocity; whether lubrication was used, what type, and where; and if inserts were used at the bar/specimen interface and a description of how they conducted bar-to-bar tests to measure interference, check bar alignment and parallelism, and how often these tests were conducted.
- **High-speed imaging setup**: The make and model of the imaging system; a picture of this setup; and the exposure time, resolution, and frame rate used.
- **Specimen information**: Specimen dimensions, temperature, and humidity at the time of each test; pulse shaper material and dimensions, if used; how the compressive strength was calculated for each specimen; determine if the fracture was valid or invalid and how this determination was made; calculate the strain rate for each test and how this was obtained; and provide high-speed movies of each test up to and including the time of fracture.

- **Participant information**: The participants' experience level with SHPB testing; a summary of the types of materials they have previously tested with an SHPB apparatus; the typical specimen geometry used and number of tests conducted; and how they determine if a test is considered valid or not.

4. Results

Participant information: The participants' experience with SHPB testing is summarized in Table 2. The five participants have a combined experience of almost 60 years using the SHPB to test a wide variety of materials. Four of the five participants had some experience testing ceramics prior to this exercise. Cuboids and cylinders were the geometries of choice for everyone, but the dimensions varied between participants and were quite different depending on the material being tested. The same was true for the number of specimens typically tested.

Table 2 Participant information

Participant	Experience (years)	Materials tested	Geometry used	No. of tests typically conducted
1	15	80% metals; 15% soft materials; 5% ceramics (first time testing ceramics in the exercise)	4-mm D × 2-mm L cylinder	3 if repeatability is good; more if not
2	8	Foams, polymers, composites; natural stone, metals, ceramics, and metamaterials	L/D = 0.25–1.5 in general; L/D = 0.05–0.25 soft; specimen/bar D = 0.6–1 concrete; 0.4–0.7 soft; 0.2–0.5 polymers and metals; 0.05–0.3 high-strength materials	4–8 metals and foams; 6–12 polymer, stone, concrete, and ceramics; 7–35 for large scatter
3	15	Mostly ductile metals but recently brittle materials	Cuboids with L/side of 0.5:1 or cylinders with L/D 0.5:1	At least 3, but for brittle materials as many as possible
4	~10	Mostly with ultra-hard ceramics (SiC, B_4C, Al_2O_3, etc.); some experience w/ Al, Al/Mg composites, steel, brass, etc., and 3D woven glass composites	Ceramics: 3 × 3 × 5 mm; Metals: 6.35-mm D × 12.7-mm L; Composites: high-rate bend tests using 6.35-12.7 × 12.7-50 × 50 plates	Typically 10/material with the intent of obtaining 6 valid tests; if necessary, more tests are done until 6 valid ones are achieved
5	~8	Steels, polymeric foams, Al_2O_3 and SiC	2.3 × 2.7 × 3.5 mm for ceramics; size chosen to have flat surface for DIC analysis	Tests are performed until 5–10 valid tests are obtained

D = diameter; L = length; DIC = digital image correlation.

SHPB apparatuses: Information on the different SHPB apparatuses used by the participants is summarized below and in Table 3, while images of the individual apparatuses can be found in Appendix B. The incident, transmission, and striker bars of each apparatus employed in this exercise were made of maraging steel, but each had different bar lengths and diameters. Participants 4 and 5 did not have a momentum trap assembly on their respective units. All of the participants routinely perform bar-to-bar tests to check bar parallelism and alignment. How often these tests were performed varied with each participant, but the overarching approach was to run tests when a new material was to be tested, when the setup was changed (addition or subtraction of strain gage(s) on a bar, bars are switched out, etc.), or when unexpected test results or wave shapes are seen that may indicate misalignment. A pulse shaper was used by everyone to ensure a constant strain rate was achieved with an appropriately ramped input pulse. Annealed copper was the preferred pulse shaper material, but aluminum (participant 3) and tin (participant 5) were also used. The size of the pulse shaper varied with each participant. All participants placed sacrificial tungsten carbide inserts (of various sizes and shapes) between the ends of the bar and the specimen to protect the ends of the bars from damage, and they all used some form of lubrication at the interfaces to minimize the effects of friction. Specific details on the individual SHPB apparatus of each participant, beyond the information in Table 3, is given in the following sections.

Table 3 Information on the participants' SHPB setup

Participant no.	Incident Transmission Striker	Momentum trap	Striker velocity (m/s)	Lubrication	Pulse shaper	Inserts
1	• All maraging steel (unhardened) • All 15-mm D • Incident and Transmission both 1500-mm L • Striker 203-mm L	15 D × 300 L steel rod in contact with transmission bar	9.9 ± 0.1	Heavy grease between bars and spherical joint; bar/WC interface	Annealed Cu: 4.64-mm D × 1.59-mm L	WC tool insert 12 mm × 12 mm × 3.22 mm
2	• All 350 maraging steel • All 25.4-mm D • Incident 3340 mm long • Transmission 1524 mm L • Striker 305 mm L	350 maraging steel; 25.4-mm D × 1524 mm long	No velocity; gun pressure 22–30 psi	High-pressure grease at WC/bar, WC/specimen and bar/pulse shaper interface	Annealed Cu: 6.35 mm D × 1.5 or 2.3 mm L	C-2 WC 15.87-mm D × 9.52-mm L
3	• All made out of C350 maraging steel • First two tests used a 6.35-mm D; remaining eight tests used a 9.53-mm D • Incident 915- and 1219-mm L • Transmission 915- and 762-mm L • Striker 101-mm L for all tests	300 mm long in first two tests then 431 mm long for remaining eight tests	Not measured	Moly grease	Al 1110; 4.8-mm D × 0.254-mm L	WC inserts on only the final eight tests
4	• All VascoMax C300 maraging steel • All 19.05-mm D • Incident and Transmission both 6096-mm L • Striker 610-mm L	None	Depends on material; 9–12 for these round-robin tests	Synthetic grease between brass bushing and bars	Annealed Cu: 7.93-mm D × 1.57-mm L	WC C2 grade 12.2-mm D × 6.35-mm L
5	• All C350 maraging steel • All 12.7-mm D • Incident 1016 mm long • Transmission 914-mm L • Striker 304.8-mm L	None	15–16 based on a gas pressure of 40 psi	High-pressure grease	Sn: 4.109-mm D × 1.609-mm L	WC jacketed with Ti-6Al-4V

D = diameter; L = length

Participant 1: This participant assumed the supplied specimens had a strength of 5 GPa (17.8-kN break load) and a fracture strain of 0.0135, based on a Young's modulus of 370 GPa. The striker bar length and impact velocity as well as the pulse shaper material and dimensions were selected based on these assumptions to provide a constant strain rate while simultaneously exceeding both the fracture load and fracture strain of the specimen. Several trial tests were conducted using spare specimens the participant had available to confirm that these parameters were appropriate for the round-robin specimens. The participant also conducted six tests

with a single 15-mm-diameter spherical joint made of maraging steel located on the transmission bar side immediately behind the tungsten carbide (WC) insert. The joint was an attempt to minimize potential misalignment that could result in an applied bending stress. A round (12-mm diameter × 3 mm thick) impedance matched WC platen with a stainless steel confining ring was used to align the specimen on the bar centerline. This platen was only used on the incident bar of four tests while square WC platens were used in all other cases. Figure 4 is a close-up of this test arrangement.

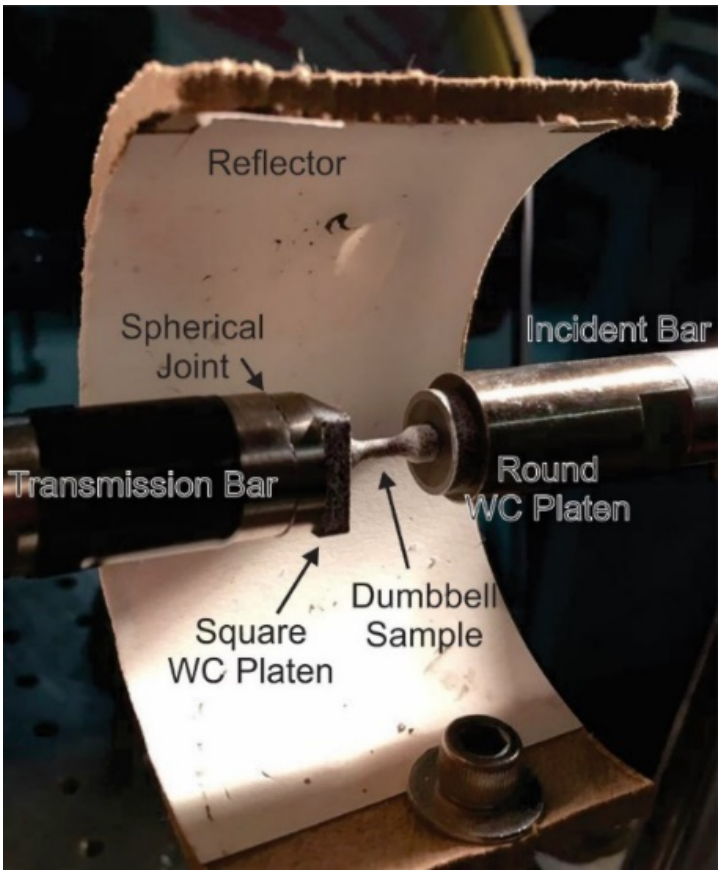

Fig. 4 Detailed image of the specimen area in the test setup used by participant 1. The spherical joint that was used in some tests can be seen on the transmission bar side.

Participant 2: Heat-shrink plastic tubing was used to hold the WC inserts in place on the ends of the incident and transmission bars as shown in Fig. 5.

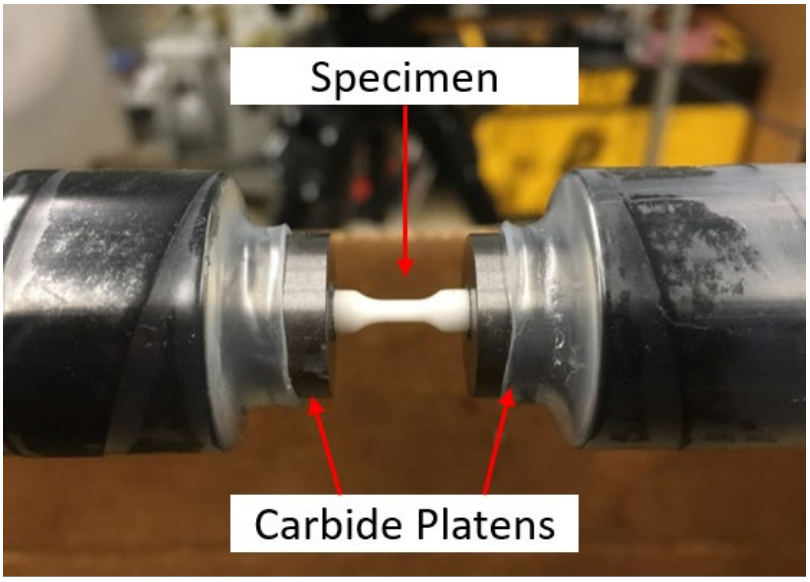

Fig. 5 Specimen setup used by participant 2 showing the heat-shrunk plastic holding the sacrificial WC inserts in place on both bars

Participant 3: The first two tests this participant conducted were deemed "invalid" due to axial splitting of the specimen and the loss of strain gages during the test. Based on these two results, the diameter of the bars in the SHPB unit was increased and WC inserts were placed at the bar/specimen interface for all future tests. Coaxial alignment of the specimen on the bars was accomplished using polycarbonate collets that were machined to have coaxially aligned inner diameters that matched the bar diameter on one side and the specimen end diameter on the other (Fig. 6). The WC inserts fit inside these alignment collets.

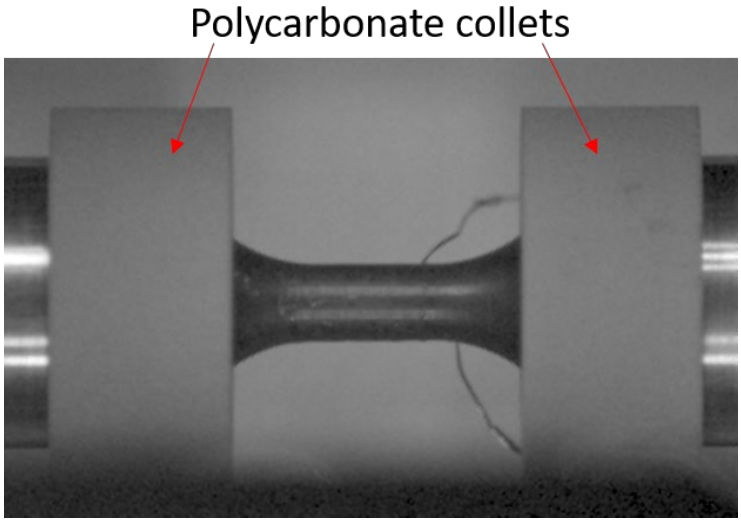

Fig. 6 Specimen setup employed by participant 3. Polycarbonate alignment collets were used to coaxially align the specimen with the bars. The wires coming off the specimen are affixed to the strain gage that is on the opposite side of the specimen and out of the field of view.

Participant 4: This participant used an SHPB apparatus that included incident and transmission bars that were each over 6 m long. These lengths were achieved by joining two, 3-m-long bars with a threaded union. Wood's metal was added to both unions to ensure a tight fit. A momentum trap was not part of the setup because video and strain gage information shows that the specimen breaks after a single pulse and because the compressive pulse that reaches the end of the transmission bar pulls the bar away before a second pulse can travel back to the end of the bar. A box was placed around the specimen area to collect the specimen fragments.

Participant 5: This SHPB apparatus was built on an optical table to minimize vibrations. WC platens, jacketed with a Ti6Al4V sleeve, were used in all tests to protect the ends of the bar from damage by the harder ceramic material. Similar to participant 4, the unit did not employ a momentum trap.

Imaging systems: It was very interesting that three of the participants used the exact same camera model to record the fracture event, but with slightly different exposure times, frame rates, and resolutions (Table 4). Participant 4 also used this same camera model for the first three tests but switched to a twin camera setup with a different camera model so 3D digital image correlation (DIC) measurements could be made. Participant 1 also employed a twin camera system, but with a different camera model than participant 4, and it had a flash unit centered over the cameras with a semi-circular diffuse reflector to improve illumination. The included angle of the cameras used by participant 1 was approximately 24° with a working distance of approximately of 250 mm.

Table 4 High-speed imaging information

Participant	Camera information	Exposure time	Frame rate (1/s)	Resolution (pixels)
1	Twin Photron SA1 CMOS; Photogenic PL2500 DR Flash w/ 90-mm lens; semi-circular diffuse reflector	1.76 μs	75,000	128 × 352
2	Shimadzu Hyper Vision HPV-X2	500 ns	500,000	400 × 250
3	Shimadzu Hyper Vision HPV-X2 w/ 200-mm lens	200 ns	1 or 2 million	400 × 250
4	Shimadzu Hyper Vision HPV-X2 (three tests) Specialized Imaging Kirana (seven tests)	200–500 ns 2 μs	1–2 million 500,000	400 × 250 924 × 768
5	Shimadzu Hyper Vision HPV-X2 w/ Infinity K2 DistaMax Lens and CF-3 Objective	400–500 ns	500,000	400 × 250

Strain rate: In all cases the strain rate was determined by fitting a straight line to the strain profile from the strain/time curve generated for each specimen. The mechanism for measuring the strain in the specimen gage section varied. DIC coupled with the strain gages on the bars was the approach four of the participants used. Participant 1 placed a speckled pattern on both WC inserts as well as the specimen while participants 2, 4, and 5 only placed the pattern on the specimen. While they all used DIC, they each examined the strain in the specimen gage section in a different manner.

The high curvature of the specimens coupled with the use of a twin camera system resulted in a very narrow correlation region on the sample (purple area in Fig. 7a), limiting the DIC data available to participant 1. As a result, the participant used a "virtual strain gage" (white box on gage section in Fig. 7a) to measure the relative displacement between two correlated subsets on the compression axis and implied a uniaxial strain state. Additionally, the participant estimated the strain rate from the overall strain on the specimen as follows:

> The strain rate during the test is estimated from the overall strain on the dumbbell specimen, as determined from the Kolsky bar strain wave analysis, and a factor representing the relation between the gage strain and the overall strain. This factor is assumed to depend only on the geometry of the specimen, and is therefore considered a constant for all tests. The gage strain factor is determined in two ways. First, a ratio of the DIC strain obtained on the gage section with that obtained using the extreme ends of the specimen is computed. For several different tests, the ratio of the DIC gage strain to the DIC overall strain was found to be 1.4. Second, a finite element analysis (FEA) is performed using an axisymmetric specimen of approximately the same dimensions as the test specimen with the exception that the transition between the specimen ends and the gage section is conical rather that curved.

The resulting gage strain to overall strain ratio was calculated as 1.4 from the DIC and 1.57 from the FEA. The DIC value was used for all strain rate determinations.

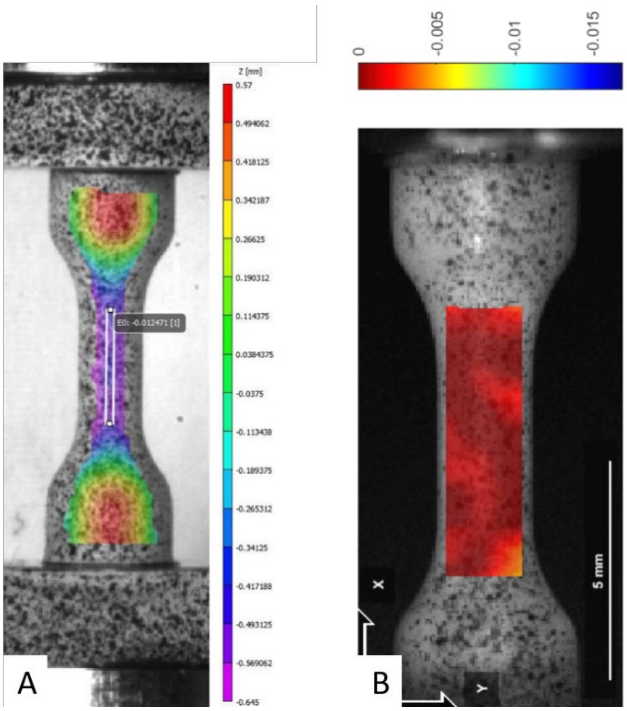

Fig. 7 DIC images from A) participant 1, with the white box representing the "virtual strain gage", and B) participant 2

Participant 2 determined the nominal strain on the specimen using the strain gages on the bars of the SHPB apparatus and determined the average strain in the specimen gage section using the area highlighted by the red box in Fig. 7b. Unlike participant 1, it appears that participant 2 did not take into account the curvature of the gage section. An alternate attempt was made by adding marker lines to define the gage section, instead of a speckled pattern, but movement of the lines was not sufficiently clear to determine the strain. Participant 4 determined the strain rate for the first three specimens only using the gages on the bars, but for the final seven tests determined the gage section strain rate using the bar gages and DIC of the specimen. The participant successfully captured strain data from five tests using both methods. Participant 5 used a different speckled pattern for their DIC measurements. The white alumina specimens were painted black, and then a silver speckled pattern was added. The participant used this method because the silver is more reflective with the lighting used in their high-speed imaging system. Participant 3 did not use DIC but instead used strain gages, one on the specimen gage section and the ones commonly located on the bars. The strain rate was determined from the strain (strain in the specimen gage section) versus time plots. The rate was always linear except for very early/low strains as reported by the participant.

Test validity: The participants considered the following questions when determining if a test was valid or invalid:

- Did fracture initiate in the specimen gage section or from axial splitting at the end faces?
- Was stress equilibrium achieved?
- Was the strain rate constant throughout the test?
- Did the specimen experience bending or rotation?

Figure 8a–d provides examples of a test where fracture initiated in the specimen gage section, and was thus deemed as a valid test, as well as a test that was considered invalid because axial cracking appeared prior to any damage forming in the gage section (Fig. 8e–g).

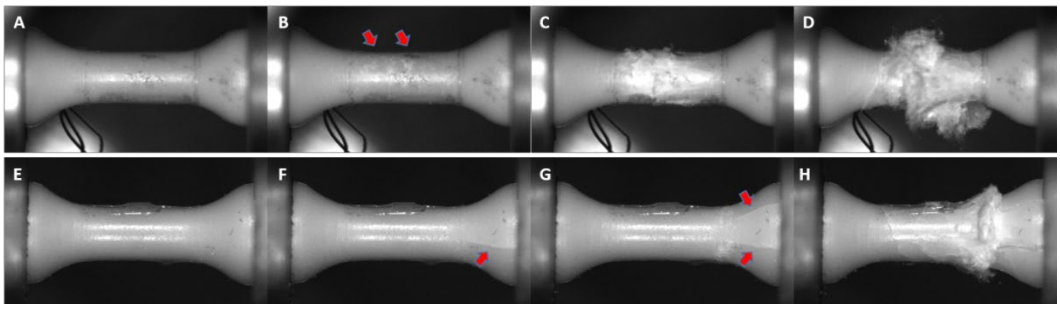

Fig. 8 Examples of a valid fracture (A–D) and an invalid fracture (E–H) from participant 3. The red arrows denote the first evidence of damage; (B) gage section of specimen that exhibited a valid fracture; and (G and H) axial cracking in a specimen that exhibited an invalid fracture. All images were taken within 3–4 μs of each other.

Strength and strain: Four of the participants determined the compression strength using Eq. 1, where σ_c = compression strength; E_b = elastic modulus of the bar material; A_b = area of the bar; A_s = area of the specimen gage section, and ε_b = maximum strain amplitude in the transmission bar.

$$\sigma_c = E_b \frac{A_b}{A_s} \varepsilon_b \quad (1)$$

The remaining participant measured the peak strain in the bar and converted this value to a peak load, which was then divided by the area of the specimen gage section to yield an engineering compressive strength value.

Table 5 summarizes the participants' results while Appendix C contains the individual data points from each participant. Each participant tested all 10 specimens provided. In some instances a component of the test setup did not function properly (e.g., strain gage malfunctioned or fell off, the camera was not

triggered to record). Such a malfunction prevented data from being collected or prevented the participant from determining where fracture initiated. These tests were considered "unsuccessful" tests and not "invalid" tests.

Table 5 Summary of test results

Participant	No. tested	No. of unsuccessful tests[a]	No. valid	No. invalid	Ave σ_c (GPa)[b]	Ave $\dot{\varepsilon}$ (1/s)[b]	Temperature (°C)	Humidity (%)
1	10	1	4	5	4.47 ± 0.16	110 ± 2.1	23-24	18 or 32
2	10	0	8	2	4.92 ± 0.20	107 ± 6	22	49
3	10	0	7	3	4.40 ± 0.50	756 ± 135	RT	Normal
4	10	2	6	2	4.42 ± 0.16	146 ± 25	20 ± 1	25 ± 10
5	10	1	5	4	4.84 ± 0.18	102 ± 20	21	Not measured

[a] A test is considered unsuccessful if a test component (strain gage, imaging system, etc.) did not function properly.
[b] The values reported with the average strength and strain rate are ± 1 standard deviation.

Participant 1 tested six specimens with a spherical joint in the transmission bar. Four of these tests were considered invalid due to specimen rotation that was observed in the high-speed video. The average strength of these invalid tests was about 15% lower (3.8 ± 0.2 GPa) than the valid results. No rotation was noted in the video of the fifth test conducted at a higher strain rate (273/s). This specimen had a strength of 4.5 GPa, but the force equilibrium was poor and thus it was also deemed invalid. The high-speed video recording failed to work properly on the sixth test, but the specimen had a resulting compression strength of 4.1 GPa. Since validity could not be confirmed, the test was deemed unsuccessful and the participant did not include the value in the average strength calculation. The participant noted that they were unable to observe specimen bending during the test due to the limited resolution of their DIC measurement system. The strain at fracture for these tests was consistently measured to be around 1.3%.

Two of the test results reported by participant 2 were classified as invalid since specimen bending was observed in the high-speed videos. The stress/nominal strain curves for these two tests were also different from the valid tests. A strength value was not provided for these specimens, but the engineering stress was below 4 GPa for both specimens based on these curves. A third test result was also in question as the participant noted that the strain rate was not as constant as the other specimens, but the strength was valid. The participant considered it a valid data point, and the resulting compressive strength value of 5.0 GPa was included in the average compressive strength calculation. Removing this result from the calculation does not change the average compressive strength determined by the

participant. The participant also determined the average elastic modulus of the material from the stress/strain curves (Fig. 9) as 398 ± 13 GPa, which is slightly higher than the reported value of 370 GPa.

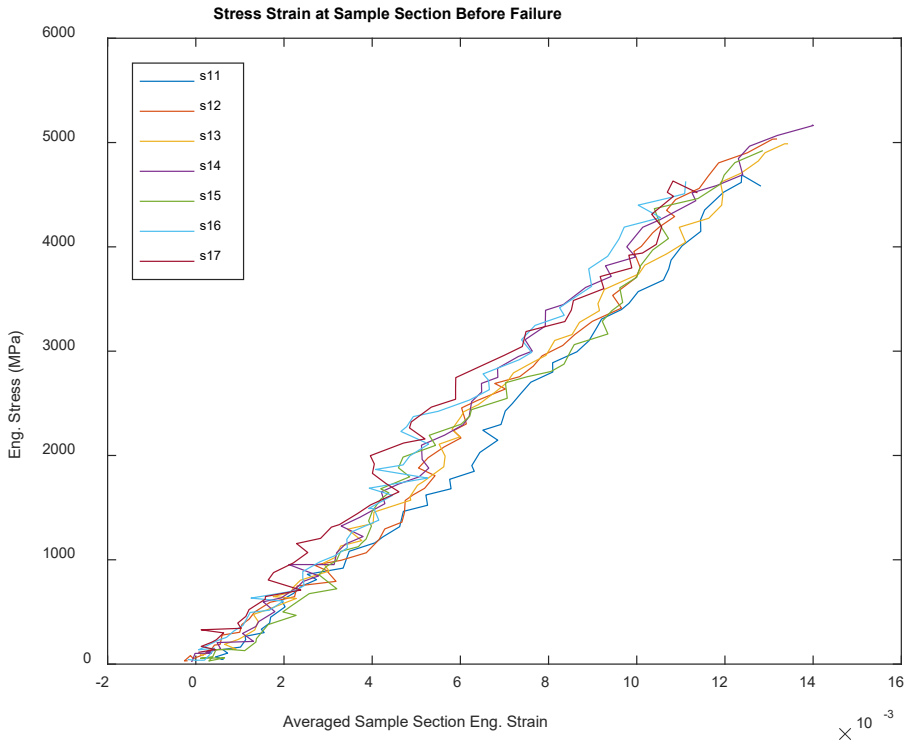

Fig. 9 Stress-strain curves generated by participant 2 used to determine elastic modulus

Participant 3 labeled three of the 10 tests conducted as invalid. Two of the three exhibited axial splitting of the dumbbell end. A compressive strength value of 4.91 GPa was determined for one specimen, but a value was not calculated for the other. No splitting was observed on the third specimen, but the strain gage was lost and there was evidence that the specimen was not in equilibrium. The strain gage was lost on a fourth specimen, but fracture was deemed valid based on the video and because the test was conducted in the same manner as all of the other valid tests; the strain rate obtained from the reflected wave was very close to all of the other valid tests, thus the strain rate was estimated based on the other valid results. Participant 3 compared the stress/strain curves to the elastic modulus from Table 1, showing that each specimen exhibited uniform elastic behavior during loading up to fracture and each had an elastic modulus that was similar to the 370 GPa value for this alumina (Fig. 10).

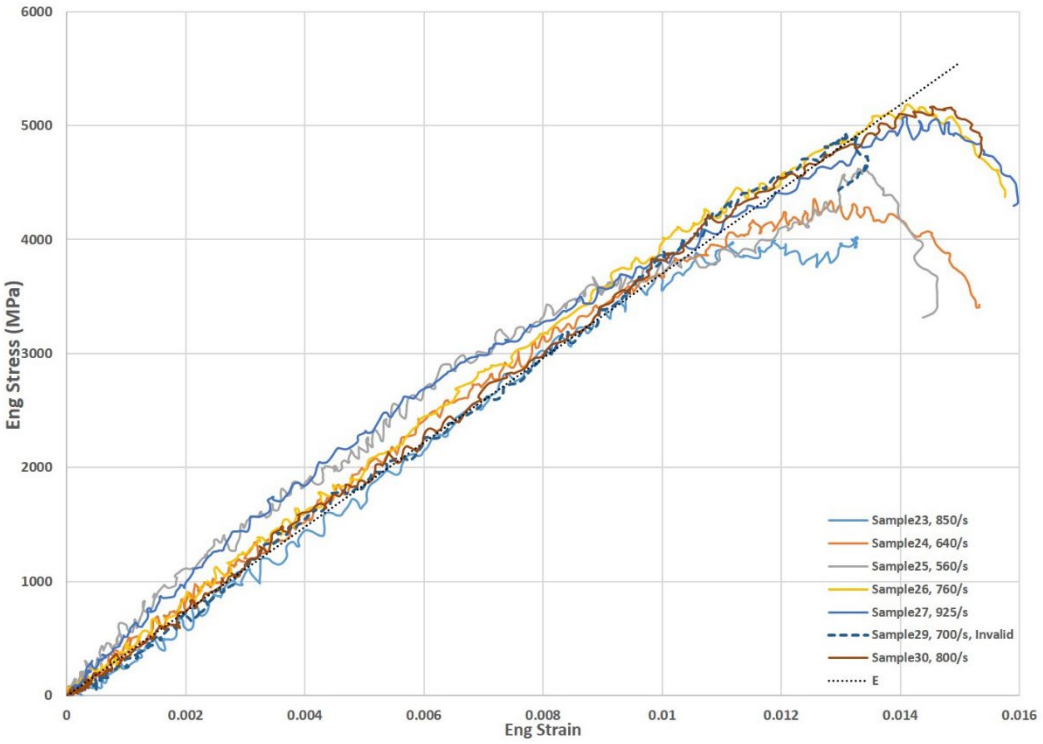

Fig. 10 Stress-strain curves generated by participant 3. The dotted "E" line has a slope of 370 GPa, the elastic modulus of the alumina from Table 1.

Equipment errors prevented data collection for two of the specimens tested by participant 4. These were deemed "unsuccessful". No video or oscilloscope data were collected on one test, and no video was collected on the second test. Despite the lack of a video, the participant believes that the second test was valid since the strain rate was consistent (175/s) and the resulting strength (4.6 GPa) is comparable to the values from the other valid tests. However, the participant did not include this data point in the average strength calculation. If this value had been included, it would not have changed the average strength value or the associated standard deviation. Six of the remaining eight tests were valid, with the two invalid tests due to axial splitting of the specimen.

Participant 5 had nine successful tests that yielded five results which were deemed valid. The one test that was not successful was the result of the gas gun misfiring. Four tests were deemed invalid due to axial splitting. This includes one specimen that exhibited both damage in the gage section and axial splitting. In this specimen the first observable damage appears in the gage section, but two frames later (~6 μs) axial cracking is observed (Fig. 11). The participant classified this as invalid because of the axial splitting coupled with a low compressive strength value (4.29 GPa) stating "the axial splitting indicates that the stress state in the specimen is not

completely compressive despite the apparent initial failure in the gage section." Inclusion of this data point would have had minimal effect on the average strength.

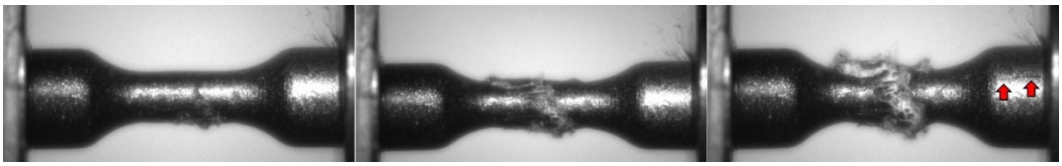

Fig. 11 Successive images (left to right) showing fracture initiating in the gage section then axial cracking (red arrows) appearing two frames later. Participant 5 deemed this an invalid result due to the axial cracking and a low compressive strength value.

Included in the five valid results from this participant was a test where a small amount of material chipped off the dumbbell end prior to final fracture (Fig. 12). The loss of this material did not seem to affect the test, as fracture still initiated in the gage section and the resulting strength value (5.08 GPa) was comparable to the other valid results.

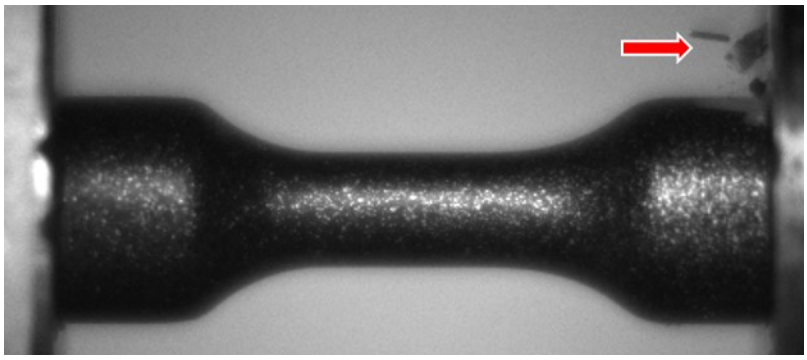

Fig. 12 Image from participant 5 showing chips (red arrow) coming off the edge of the dumbbell prior to fracture. Fracture occurred shortly after and began in the gage section so it was considered valid.

Participant 5 also showed that there was consistency between the DIC strain profiles and the stress profiles obtained from the strain gages on the bars (Fig. 13) and consistency in the stress-strain profiles (Fig. 14). The five valid test results yield an average elastic modulus of 375 ± 15 GPa, which is in excellent agreement with the reported value for this alumina.

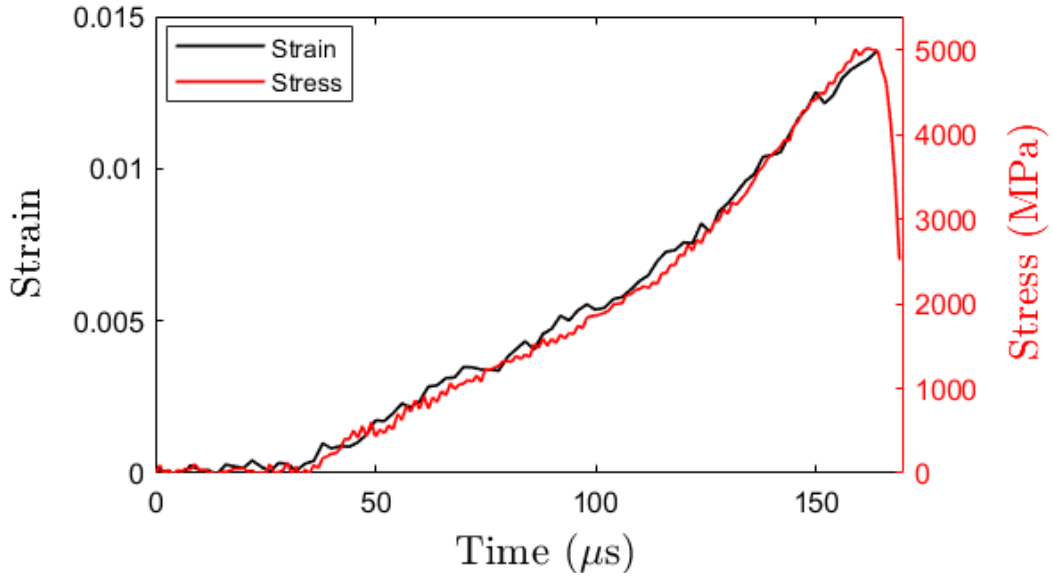

Fig. 13 Stress and strain profiles from one specimen tested by participant 5

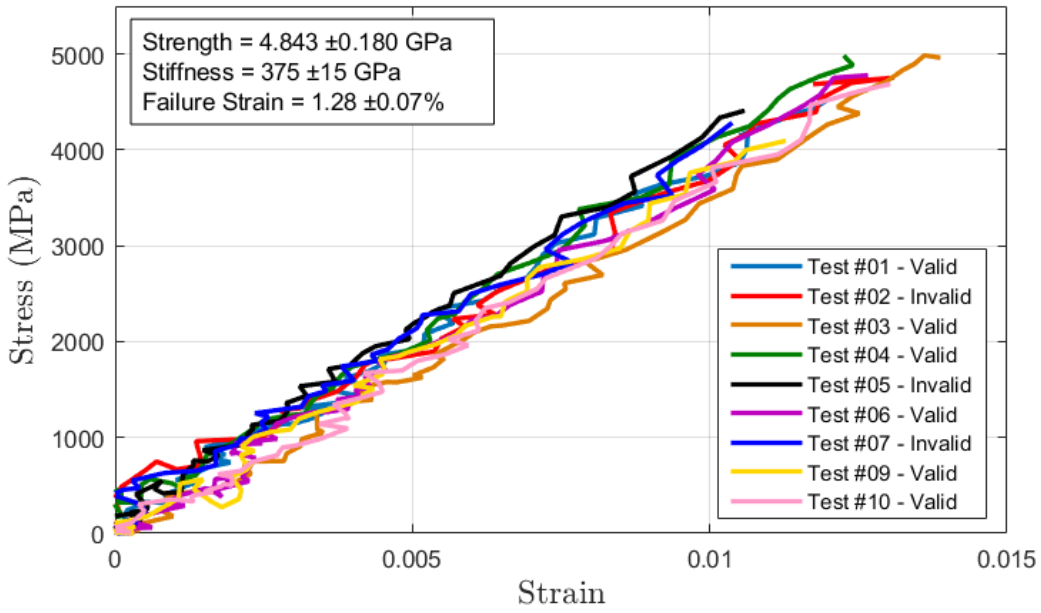

Fig. 14 Stress-strain profiles from the nine specimens tested by participant 5

5. Discussion

Strength: The average dynamic compressive strength values in Table 5 are remarkably consistent, especially considering the small number of specimens tested and the distinctly different SHPB apparatuses that were used. The success rates are impressive as well. High-speed imaging was crucial to successful testing. The grand average dynamic compression strength of this alumina, based on the average of the

unweighted five lab averages, is 4.61 GPa ± 0.25 GPa. The grand average of all 30 individual valid results from all laboratories is 4.62 GPa ± 0.36 GPa.

Quasi-static tests were also conducted on this alumina to serve as a baseline value. The same specimen geometry was tested following the procedures and guidelines in ASTM C1424*. The resulting average compression strength for 19 successful tests was 3.51 GPa ± 0.13 GPa, which is approximately 20% lower than the SHPB grand average. However, this quasi-static value is about 30% higher than the quasi-static values reported by Lankford et al.[38] for AD995 alumina and provided by CoorsTek on their website for CAP3 (Table 1). In both of these latter cases, right cylindrical specimens were tested.

The average compression strength value from each participant is plotted in Fig. 15 along with data generated on AD995 by Lankford et al.,[38] Luo and Chen,[39] and Jiao et al.[10] The difference between the quasi-static and SHPB strength shows that the compressive strength of CAP3 alumina is strain-rate dependent. Lankford et al.[38] reported a strain rate effect for AD995, but the trend is different primarily because of the significant difference in the quasi-static strength values (Fig. 15). Additionally, these authors regrettably did not provide the dimensions of the cylinders, the number of tests conducted, how the specimen fractured, or any information on the validity of the tests. Figure 16 shows additional quasi-static and dynamic results obtained by Cosculluela et al.[30] on a different high alumina: Degussa AL23 99.7% alumina. They used both dumbbell specimens (11 mm long by 7-mm gage length that was 4 mm in diameter) and cylinders (10-mm diameter by 20 mm long). A clear strain rate effect, having the same trend as our effort, is shown. It also shows that the dumbbell geometry yields a higher compression strength value than cylinders under quasi-static loading conditions. Unfortunately, the authors could not determine the strength of the cylinders at high strain rates as their SHPB unit could not achieve the load necessary to initiate fracture.

* ASTM C1424. *Standard Test Method for Monotonic Compressive Strength of Advanced Ceramics at Ambient Temperature*. West Conshohocken (PA): ASTM International.

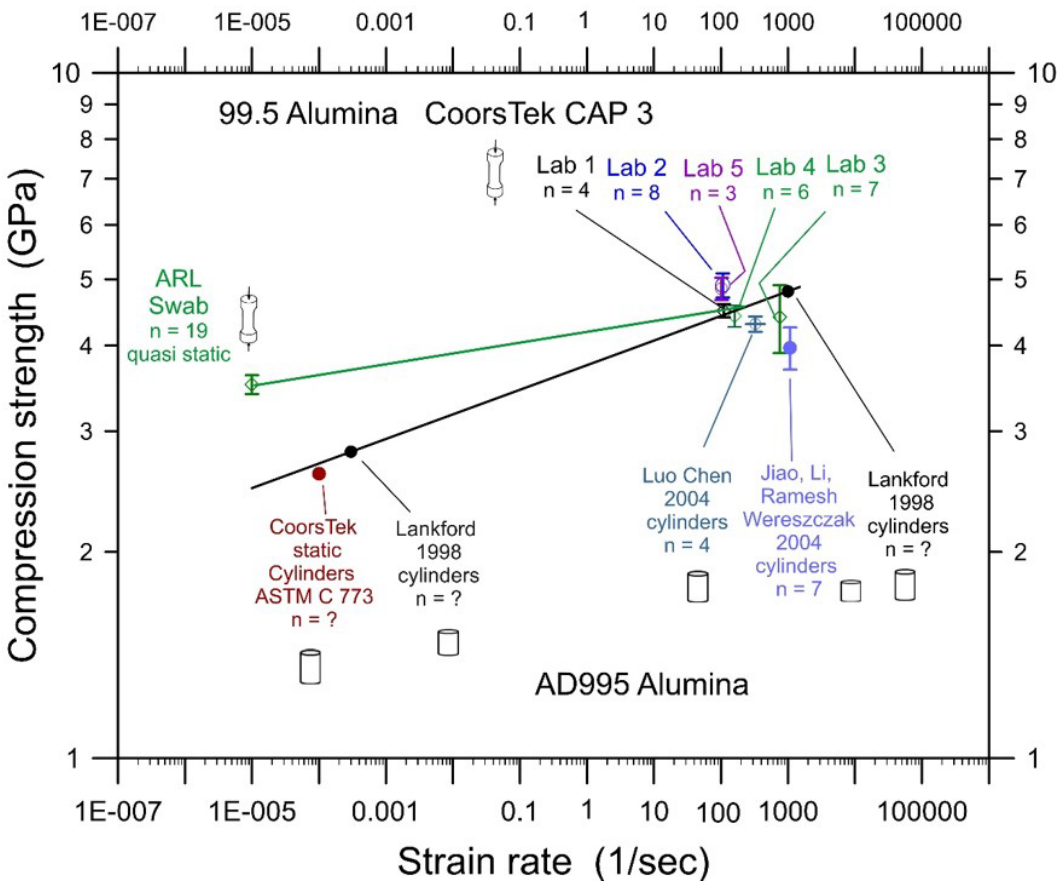

Fig. 15 Compression strength as a function of strain rate for the CoorsTek CERASHIELD CAP3 and AD995 alumina. The error bars are ±1 standard deviation.

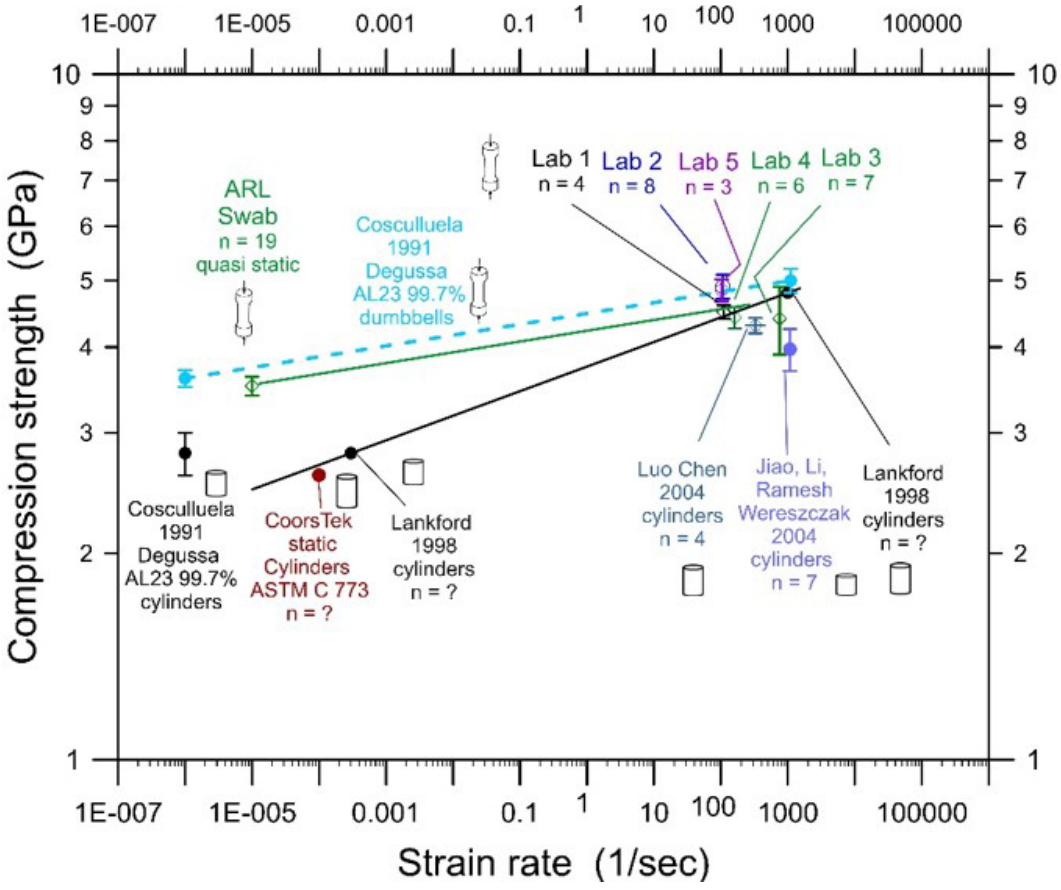

Fig. 16 Compression strength of high-purity aluminas

Other compression strength data for high-purity aluminas is scattered through the literature. For example, Swab (unpublished data) conducted quasi-static compression strength tests on a high-purity (99.9%) alumina (Coors AD999) using the same dumbbell specimen geometry used in this exercise. The average compression strength was 3.63 GPa with a standard deviation of 0.24 GPa for five specimens. This is remarkably similar to the 3.51 GPa ± 0.13 for 19 specimens obtained for the CAP3 as noted in Figs. 15 and 16. Although it was a different material (AD999 versus CAP 3), almost identical strengths were obtained.

The invalid outcomes are also of interest. When determining if a test was valid or invalid, the participants primarily focused on whether fracture initiated in the specimen gage section or elsewhere on the specimen. There were a total of 16 tests the participants classified as invalid (Table 6), with axial splitting being the most frequent reason. In the past, before high-speed photography became commonplace, judgments as to whether a test was valid or not often depended on guesswork. With quasi-static testing, intact ends of the dumbbell were good indicators of a gage section–initiated fracture as opposed to end splitting. That was how Tracy[21,22] and Dunlay et al.[23] evaluated their tests. High-speed imaging eliminates much of the

guesswork. The strength of the eight tests that were deemed invalid due to axial splitting varied significantly with several values well within the range of the average strength values from the participants' valid tests. No matter the strength value, if axial splitting occurred, the participant considered the test invalid and the datum was excluded.

Table 6 Summary of compressive strength values for the different types of invalid tests

Compressive strength (GPa)			
Axial splitting	**Specimen bending**	**Specimen rotation**	**Lack of force equilibrium**
4.91	<4	3.7	4.5
2.5	<4	3.53	---
2.4		3.79	
4.752		4.04	
4.477			
4.282			
4.096			

--- unable to determine

The importance of where fracture initiated in determining test validity is further supported by four specific results from the participants. Participant 2 had one test where the stress was acceptable and fracture initiated in the gage section, but the strain rate was not as constant as their other valid tests. Even though the rate was not constant, the test was considered valid. Similarly, the stain gage fell off the specimen during one of the tests conducted by participant 3. The datum was deemed valid because fracture initiated in the gage section. Participant 4 had a test that yielded an acceptable strength value, but because of an equipment malfunction, the fracture process was not captured. The result was not considered valid or invalid, and the datum was not included in their analysis. Finally, participant 5 observed fracture of the gage section first, then axial cracking approximately 6 μs later. The strength value was low, but acceptable, yet it was deemed invalid because the stress state may not have been completely compressive. It is also possible that the axial cracking actually occurred first but on part of the specimen away from the camera location, making it appear that the gage section fractured first. Several of the participants noted how critical it was to have a high-quality imaging system to capture the fracture process and verify the validity of a test.

The swivel joint participant 1 incorporated into their SHPB setup for four of their tests created problems. These four tests were invalid since high-speed imaging

detected rotation at the swivel joint, which resulted in rotation of the specimen. The strength values from these four tests were 4 GPa or less, and the resulting stress-strain curves were in poor agreement with the CAP3 elastic modulus of 370 GPa. However, the participant noted that the bar wave data for these invalid tests was very similar to the wave data from the valid tests. Participant 1 completed their testing without the swivel joint and obtained four valid tests with their remaining specimens. (Rotation can only be detected and measured by a two-camera DIC imaging system, as measurements made with a single camera system will ignore any motion, such as rotation, not in the image plane of the camera unless that motion is significant and visually obvious. Participants 1 and 4 were the only participants to use a two-camera imaging system and thus would have been the only participants able to observe and measure specimen rotation.)

Other factors, such as whether the specimen experienced bending or rotation, or if force equilibrium or a constant strain rate was achieved, were also considered when making the decision, but these were secondary factors. Bending was observed in two specimens by participant 2 while participant 1 noted that they did not have sufficient data to verify bending. The lower strength values when the specimen experiences bending are not surprising because of the undesirable tensile stress that will be introduced. Rotation may also introduce a tensile stress, but the specifics of this stress state will depend on how rotation occurs across the specimen.

Strain rate: The data from this round robin, and that of Lankford et al.[38], Cosculluela et al.[30], and others, indicate that ceramic compressive strengths are sensitive to strain rate, but the trends only emerge when the strain rate varies over many orders of magnitude. A factor of 2 or even 5 variation in strain rate has a minor effect. Hence, variations in strain rate within a particular test may have only a secondary effect. Figures 17, 18, and 19 are examples of strain/time curves provided by participants 2, 3, and 5, indicating how the strain can vary with time and result in different strain rates. Operator experience may also influence how the strain is determined based on the data selected for the determination.

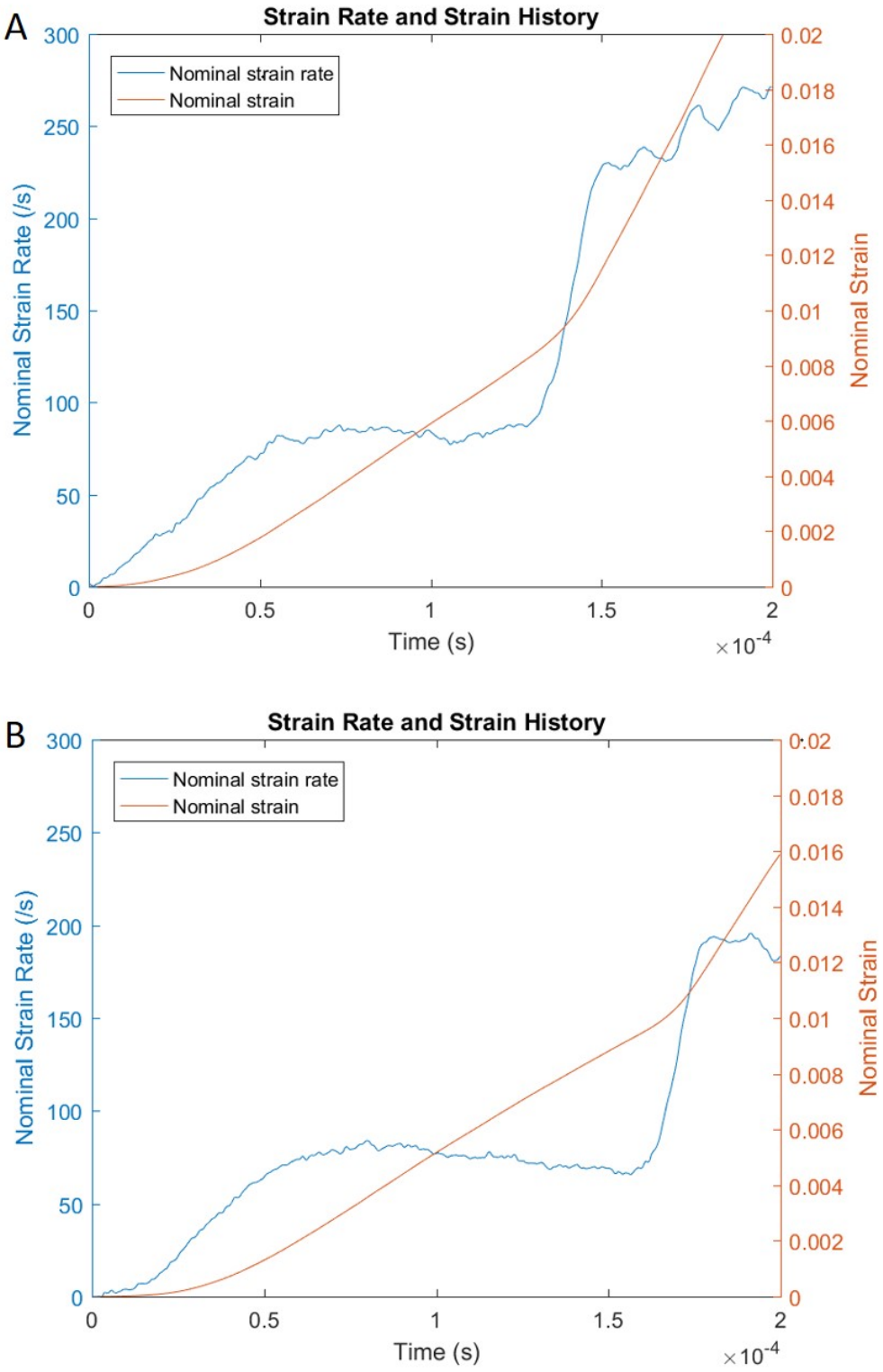

Fig. 17 Example of strain/time curves from participant 2. A) shows a nearly constant (flat) strain rate between 0.5 and 1.4 × 10^{-4} s, as determined by the participant, beyond which the strain rate dramatically increases when the specimen fractures, while in B) the participant deemed that the curve, over that same time period, was not as flat, and hence the strain rate was not as constant. The strength data from both of these specimens was considered valid.

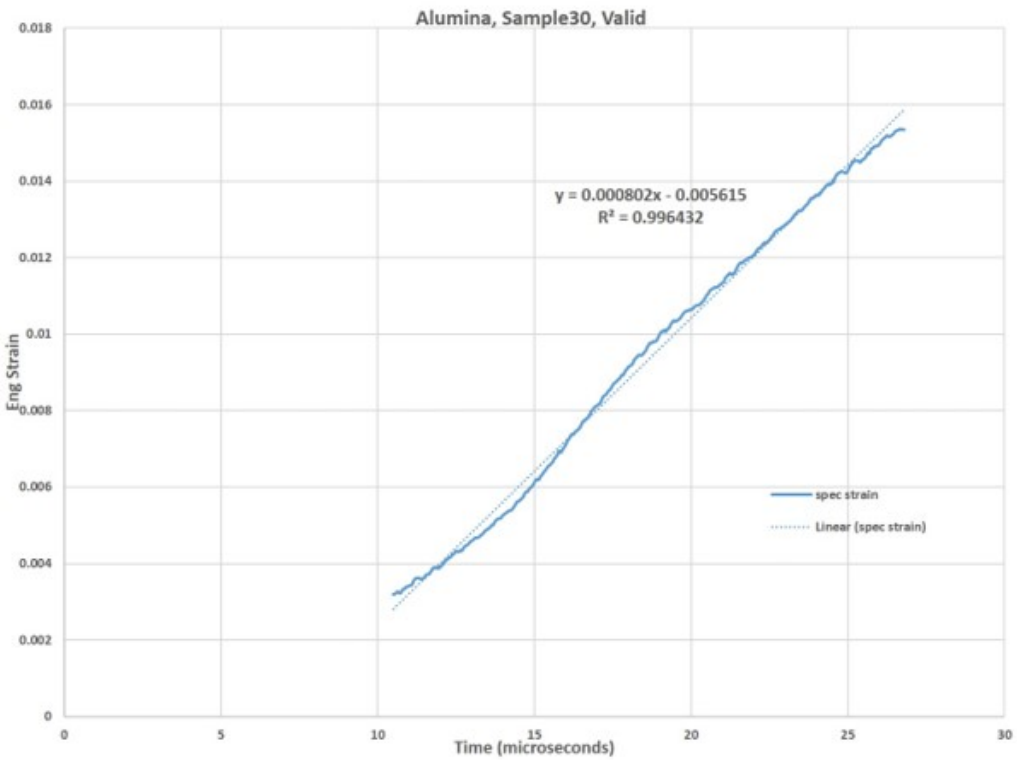

Fig. 18 A strain/time curve from a valid specimen tested by participant 3

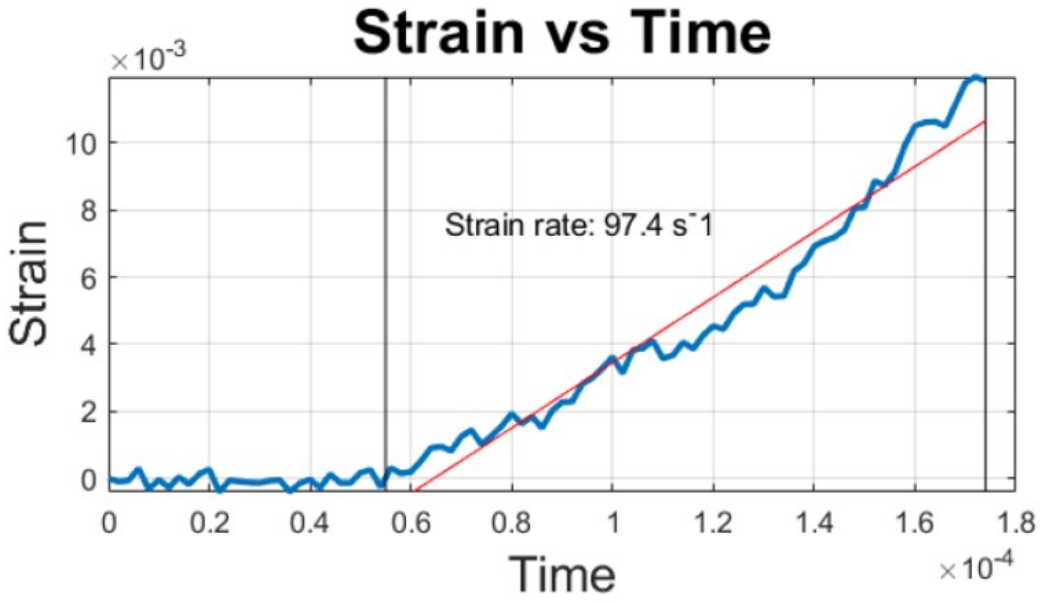

Fig. 19 An example of the strain/time curve from participant 5 with the red line showing how they determined the strain rate

Does axial splitting always result in an invalid test? Two additional studies[38,39] determined the high-strain-rate compression strength of AD995 in an SHPB apparatus using cylinders of different dimensions. In both cases, the measured compression strength was about 4 GPa, which is at the low end of the strength values obtained in this study. Given the small specimen sizes used in both cases, it is unlikely that specimen bending occurred. Test validity is not discussed in either study, but a series of images from high-speed photography is provided in one of the studies showing an axial crack in the specimen.[10] This crack forms at the specimen/bar interface and propagates the entire length of the specimen well before the peak stress is reached. While this indicates that the axial cracking was not sufficient to completely compromise the structural integrity of the specimen, it clearly demonstrates that a lateral tensile stress and not a uniaxial compressive stress was dominant. This may explain why some of the invalid tests that exhibited axial splitting in this exercise had strength values comparable to the valid test results. Similar observations were reported in boron carbide when comparing the strength obtained from cylinders to the *invalid* results obtained with the dumbbell geometry.[31] The preponderance of data from this and other studies shows that axial splitting is undesirable. While it may not always result in lower compression strengths, it clearly shows that the specimen is not failing due to a compressive stress. Thus, it is highly recommended that data from such failures be censored from the strength calculation; however, the data should still be reported as part of the findings.

The average strain rate data in Table 5 shows that there is a noticeable difference in the average reported by participant 3 (≈ 750/s) compared to the other four participants (between 100/s and 150/s). This may be due to a difference in loading time. Participants 2 and 5 had load times around 100–150 μs (Figs. 17 and 19) while participant 3 had shorter times around 25 μs (Fig. 18). Using a shorter load time will lead to a higher strain rate, but it can compromise the ability to achieve equilibrium in the specimen and thus may account for the higher standard deviation associated with the strength reported by participant 3 compared to the other participants. The most important point is that strain rate effects are typically measured over orders of magnitude; thus, while strain rates of 750/s and 150/s may seem quite different, they differ by a factor of 5; the effect of this difference on the dynamic strength, as discussed previously, is minimal. Furthermore, participant 5 successfully captured strain data from both strain gages on the bars (173/s) and DIC of the specimen gage section (159/s) that were in excellent agreement. Based on these results, as well as the information in Figs. 17–19, different methods of determining the strain rate during an SHPB test can be used and yield strain rates of comparable magnitude.

The results of this round-robin exercise clearly show that the dumbbell-shaped specimen geometry is the appropriate specimen to use when testing ceramics materials at high strain rates using the SHPB method. Consistent strength values can be obtained using a wide range of SHPB apparatuses that have different size bars, use different methods to determine the strain rate, and use different systems to capture the fracture process. However, it is essential that a high-quality high-speed imaging system be used to capture the fracture process to enhance the ability of the operator to properly identify where fracture initiated to ensure that fracture was due to a compressive and not a tensile stress.

Statistical analysis: Although it was not our original intention to conduct a rigorous statistical analysis of the data, the positive results lent themselves to a precision uncertainty analysis in accordance with ASTM standard E691* and ISO 5725-2†. Uncertainties in general are composed of both "precision" and "accuracy" (or bias) uncertainties. ASTM E691 and ISO 5725-2 use an identical procedure to evaluate precision, which is the variability (scatter) in results for test methods both *within a laboratory* and *between laboratories*. They do not deal with accuracy or bias, which is the uncertainty associated with obtaining a "true" or "reference" property value.

"Repeatability" is the variation in results obtained with one method on identical material *in the same laboratory* by the same operator using the same equipment within short intervals of time. One way of expressing it is as the *repeatability standard deviation,* which is the standard deviation of test results obtained in the laboratory. Each laboratory will have its own variability, and E691 integrates all the within-laboratory variabilities to arrive at a grand or typical "within-lab" repeatability. This can alternatively be expressed as the repeatability coefficient of variation (COV) that is the grand repeatability standard deviation normalized by the grand average value of the property.

"Reproducibility" is also a measure of precision uncertainty but is the variation in results obtained with the same method on the same material *in different laboratories* with different operators using different equipment. It also can be expressed as a standard deviation or as a coefficient of variation. It reflects the differences in test results obtained in different laboratories. Not surprisingly, the between-lab reproducibility uncertainty is usually larger than the within-lab precision uncertainty.

---

* ASTM E691-18. *Standard Practice for Conducting an Interlaboratory Study to Determine the Precision of a Test Method.* West Conshohocken (PA): ASTM International. Annual Book of Standards, Vol. 14.05.

† ISO 5725-2. *Accuracy (Trueness and Precision) of Measurement Methods and Results – Part 2: Basic Method for the Determination of Repeatability and Reproducibility of a Standard Measurement Method.* Geneva (Switzerland): International Organization for Standards, 1994.

Table 7 shows the results for this interlaboratory exercise, also known as a round robin, as calculated according to ASTM E691. (ISO 5725-2 uses the same procedure.) At first it may be a little worrisome that some laboratories in this round robin had only three or four valid outcomes, but this is not a problem. E691 includes primary examples with only three test results per laboratory. We were not in strict accord with E691, which requires no less than six laboratories for a proper interpretation. As noted previously, this exercise was started as a "mini-round robin" and not intended to produce a rigorous precision and accuracy assessment for a carefully prescribed procedure. Nonetheless, the results do lend themselves to a precision analysis as follows.

Table 7 Precision uncertainty values as evaluated by ASTM E691-18.*

Grand average compression strength	Within-lab Repeatability precision			Between-lab Reproducibility precision		
	Repeatability standard deviation	Repeatability coefficient of variation (COV)	Repeatability 95% limit[a]	Reproducibility standard deviation	Reproducibility coefficient of variation (COV)	Reproducibility 95% limit[b]
4.61 GPa	0.27	5.9%	16.7%	0.35 GPa	7.7%	21.5%

[a] 2.8 times the repeatability coefficient of variation.
[b] 2.8 times the reproducibility coefficient of variation.

The grand average in column 1 of Table 7 is the average of the laboratory means (without weighting for the number of valid tests each lab obtained.) The E691 computed repeatability standard deviation of 0.27 GPa is an estimate of the variability a given laboratory might obtain when doing a series of tests. This estimate is calculated from the five individual standard deviations obtained by the laboratories. It includes variability within the material itself as well as the operator-laboratory testing variability. In this case, the 0.27 GPa is small with respect to the grand average compression strength and, when expressed as a coefficient of variation, is only 5.9%. The 95% confidence interval is obtained by multiplying this value by a coverage factor of 2.8, giving a 95% variation confidence interval of 16.7%. In other words, 95% of the time a laboratory can expect to obtain a *single* test outcome that is within 16.7% of the mean.

The reproducibility results in Table 7 can be similarly interpreted. The values are greater, reflecting additional variability when multiple laboratories are involved. This is typical. The reproducibility standard deviation is only 0.35 GPa, or 7.7%, and the 95% confidence interval is ±22%. These values are not that much larger

* One complication was that the laboratories had differing numbers of valid tests: four to eight. For the E691 calculations, each laboratory's average strength and standard deviation were individually calculated and weighted the same as for values from the other laboratories. This does not affect the calculated repeatability or reproducibility values.

than the within-laboratory uncertainties, which is a very positive outcome. In other words, different laboratories can obtain fairly consistent results with each other.*

6. Conclusions

This round-robin exercise answered the three questions posed originally:

1) Is the dumbbell shape the appropriate specimen geometry for testing high strength ceramics using the SHPB method?

2) Can consistent compression strength values be obtained using the dumbbell specimen?

3) Are there any potential issues related to the testing of these specimens in the SHPB?

A dumbbell-shaped specimen is eminently suitable for testing ceramics using the SHPB method. Success rates were very good and will likely increase as users gain more experience. Consistent compression strength values were obtained with this specimen geometry. Minor issues related to testing these ceramic specimens in the SHPB were identified.

The five participants were each provided with 10 dumbbell-shaped specimens of a commercially available alumina. Using their unique SHPB apparatuses, the participants obtained very comparable compressive strength values between 4.40 and 4.92 GPa. High-speed imaging was required to capture the fracture process and provided the operator with the ability to verify that fracture initiated in the gage section of the specimen due to a compressive stress. Different methods were used to obtain strain data, but all yielded strain rates on the order of 10^2/s. The results from this exercise clearly show that the dumbbell shape is appropriate and provides consistent compressive strength values irrespective of the details associated with the individual SHPB apparatuses.

* A rigorous uncertainty evaluation would need more laboratories ($n \geq 6$), a more rigorously defined test protocol, and probably multiple specimen sizes and even different materials. Nonetheless, the results obtained so far are very encouraging.

7. References

1. Crouch IG, editor. The science of armour materials. Cambridge (UK): Woodhead Publishing; 2017.
2. Meyers MA. Dynamic behavior of materials. New York (NY): John Wiley and Sons, Inc.; 1994.
3. Ramesh KT. High strain rate and impact experiments. In: Handbook of experimental solid mechanics. 2008;1–30.
4. Ravichandran G, Subhash G. Critical appraisal of limiting strain rates for compression testing of ceramics in a split Hopkinson pressure bar. J Am Ceram Soc. 1994;77(1):263–267.
5. Staehler JM, Predebon WW, Pletka BJ, Lankford J. Testing of high-strength ceramics with split Hopkinson pressure bar. J Am Ceram Soc. 1993;76(2):536–538.
6. Lankford J. Mechanisms responsible for strain-rate-dependent compressive strength in ceramic materials. J Am Ceram Soc. 1981;2:C33–C34.
7. Ramesh KT, Ravichandran G. Dynamic behavior of a boron carbide-aluminum cermet: experiments and observations. Mech Mat. 1990;10:19–29.
8. Subhash G, Ravichandran G. Mechanical behavior of a hot pressed aluminum nitride under uniaxial compression. J Mat Sci. 1998;33:1933–1939.
9. Wang H, Ramesh KT. Dynamic strength and fragmentation of hot-pressed silicon carbide under uniaxial compression. Acta Mater. 2004;52:355–367.
10. Jiao T, Li Y, Ramesh KT, Wereszczak AA. High rate response and dynamic failure of structural ceramics. Int J Appl Ceram Technol. 2004;1(3):243–253.
11. Paliwal B, Ramesh KT, McCauley JW. Direct observation of the dynamic compressive failure of a transparent polycrystalline ceramic (AlON). J Am Ceram Soc. 2006;89(7):2128–2133.
12. Farbaniec L, Hogan JD, Ramesh KT. Micromechanisms associated with the dynamic compressive failure of hot-pressed boron carbide. Scripta Mater. 2015;106:52–56.
13. Farbaniec L, McCauley J, Hogan J, Ramesh K. Anisotropy of mechanical properties in a hot-pressed boron carbide. Int J Appl Ceram Technol. 2016;1–9.
14. Chen W, Rajendran AM, Song B, Nie X. Dynamic fracture of ceramics in armor applications. J Am Ceram Soc. 2007;90(4):1005–1018.

15. Chen W, Ravichandran G. Failure mode transition in ceramics under dynamic multiaxial compression. Int J Fract. 2000;101:141–159.

16. Chen W, Ravichandran G. Dynamic compressive failure of a glass ceramic under lateral confinement. J Mech Phys Sol. 1997;45(8):1303–1328.

17. Casem DT, Dwivedi AK, Swab JJ, Wright JC, Mondal AB. Analysis of a three-bar Kolsky apparatus for high-rate three-point flexure. J Dyn Behav Mater. 2015;(1):75–93.

18. Koeppel BJ, Subhash G. Characteristics of residual plastic zone under static and dynamic Vickers indentations. Wear. 1999;224:56–67.

19. Hanner LA, Pittari JJ III, Swab JJ. Dynamic hardness of cemented tungsten carbides. Int J Ref Metals Hard Mat. 2018;75:294–298. https://doi.org/10.1016/j.ijrmhm.2018.05.007.

20. McCauley JW, Quinn GD. Special workshop: Kolsky/split Hopkinson pressure bar testing of ceramics. Aberdeen Proving Ground (MD): Army Research Laboratory (US); 2006. Report No.: ARL-SR-144.

21. Tracy CA. A compression test for high strength ceramics. J Test Eval. JTEVA. 1987;15(1):14–19.

22. Tracy C, Slavin M, Viechnicki D. Ceramic fracture during ballistic impact. In: Fractography of glasses and ceramics. Westerville (OH): American Ceramic Society; 1988. pp. 295–306. (Advances in ceramics; vol. 11).

23. Dunlay WA, Tracy CA, Perrone PJ. A proposed uniaxial compression test of high strength ceramics. Watertown (MA): Army Materials Technology Laboratory (US); 1989. Report No.: MTL TR 89-89.

24. Sines G, Adams M. Compression testing of ceramics. In: Fracture mechanics of ceramics. New York (NY): Plenum Press; 1978. pp. 403–449. Vol. 3.

25. Birch JM, Wilshire BD, Owen JR, Shantaram D. The influence of stress distributions on the deformation and fracture behavior of ceramic materials under creep conditions. J Mat Sci. 1976;11:1817–1825.

26. Bortz SA, Burton KT. Analysis and review of mechanical testing procedures for brittle materials. In: Structural ceramics and design. New York (NY): Gordon and Breach; 1969. pp. 95–98.

27. Blumenthal WR, Gray GT III. Response of aluminum-infiltrated boron-carbide cermets to shock-wave loading. J Mat Sci. 1994;29:4567–4576.

28. Blumenthal WR. High strain rate compression testing of ceramics and ceramic composites. In: Swab JJ, editor. Advances in Ceramic Armor: A Collection of Papers Presented at the 29th International Conference on Advanced Ceramics and Composites; 2005 Jan 23–28; Cocoa Beach, FL. The American Ceramic Society; c2005. (Ceramic Engineering and Science Proceedings; vol. 26, no. 7.)

29. Pickup I. The correlation of microstructural and mechanical characteristics of silicon carbide with ballistic performance. In: Swab JJ, editor. Advances in Ceramic Armor: A Collection of Papers Presented at the 29th International Conference on Advanced Ceramics and Composites; 2005 Jan 23–28; Cocoa Beach, FL. The American Ceramic Society; c2005. (Ceramic Engineering and Science Proceedings; vol. 26, no. 7.)

30. Cosculluela A, Cagnoux J, Collombet F. Uniaxial compression of alumina: structure, microstructure, and strain rate. J Phys IV. 1991(1):C3-109–C103-116.

31. Swab JJ, Meredith CS, Casem DT, Gamble WR. Static and dynamic compression strength of hot-pressed boron carbide using a dumbbell-shaped specimen. J Mat Sci. 2017;52:10073–10084. DOI 10.1007/s10853-017-1210-7.

32. Chen W, Subhash G, Ravichandran G. Evaluation of ceramic specimen geometries used in split Hopkinson pressure bar. DYMAT Journal. 1994;1(3):193–210.

33. Hogan JD, Farbaniec L, Sano T, Shaeffer M, Ramesh KT. The effects of defects on the uniaxial compressive strength and failure of an advanced ceramic. Acta Mat. 2016;102:263–272.

34. Farbaniec L, Hogan JD, Xie KY, Shaeffer M, Hemker KJ, Ramesh KT. Damage evolution of hot-pressed boron carbide under confined dynamic compression. Int J Imp Eng. 2016;99:75–84.

35. Farbaniec L, McCauley J, Hogan J, Ramesh K. Anisotropy of mechanical properties in a hot-pressed boron carbide. Int J Appl Ceram Tech. 2016;1–9.

36. Ghosh D, Subhash G, Zheng JQ, Halls V. Influence of stress state and strain rate on structural amorphization in boron carbide. J Appl Phys. 2012;111(6):063523.

37. Wereszczak AA, Swab JJ, Kraft RH. Effects of machining on the uniaxial and equibiaxial flexure strength of CAP3 AD-995 Al_2O_3. Aberdeen Proving Ground (MD): Army Research Laboratory (US); 2015 Sep. Report No.: ARL-TR-3617.

38. Lankford J, Predeon WW, Staehler JM, Subhash G, Pletka BJ, Anderson CE. The role of plasticity as a limiting factor in the compressive failure of high strength ceramics. Mech Mater. 1998;29:205–218.

39. Luo H, Chen W. Dynamic compressive response of intact and damaged AD995 alumina. Int J Appl Ceram Technol. 2004;1(3):254–60.

Appendix A. Instructions and Participant Questionnaire

This appendix appears in its original form, without editorial change.

Mini-Round Robin on SHPB Testing of Advanced Ceramics

Purpose:

Determine if the dumbbell-shaped specimen is the appropriate geometry for determining the dynamic compression strength of advanced ceramics using a Split Hopkinson Pressure Bar (SHPB) set-up

Material:

- CoorsTek CAP3 Al_2O_3
- 10 dumbbell-shaped specimens

Testing Instructions:

1) Determine the dynamic compression strength of each specimen using a Split Hopkinson Pressure Bar. Target is 3-5 valid tests (preferably 5)
2) Determine the strain rate for each specimen tested
3) Use high-speed imaging to capture the fracture process

Data/Information Required:

1) Information on the SHPB set-up:
    a) Dimensions (diameter and length) of the striker, incident and transmission bars
    b) Striker, incident and transmission bars material(s)
    c) Picture of the entire SHPB set-up
    d) Brief description of the set-up and testing procedures
    e) Strain rate measurement method (strain gage(s), digital image correlation, etc.)
    f) Do you conduct bar-to-bar tests to measure interference as well as bar parallelism and alignment? Provide a description of how these tests are conducted and how often they are conducted.
    g) Is lubrication used in the system?
    h) Do you know the striker bar velocity? If so, please provide this value.
2) Information on the high-speed imaging set-up:
    a) Exposure time

b) Resolution

c) Frames/second

d) Picture of the high-speed imaging system

e) Make and model of imaging system (optional)

3) Information for each specimen tested:

a) Dimensions of the specimen

b) Temperature and humidity at the time of each test

c) Was a pulse shaper used? If so, provide pulse shaper material and dimensions

d) Calculate the compressive strength of each specimen

e) Determine if fracture was considered valid or invalid based on the fracture process

f) Calculate the strain rate for each test

g) How was the strain rate determined for each test?

h) Provide high-speed movies (preferred) for each specimen up to and including the time of fracture. **NOTE**: Due to the size of these files I will request a "drop-off" using the ARL SAFE (Secure Access File Exchange) system when these files are ready to be sent.

Participant Information:

1) What is the participants' experience level with the SHPB method?

2) What materials has the participant tested previously using the SHPB method?

3) What is the typical specimen geometry used to test the materials listed in item 2)? (EX. Cuboidal specimen nominally A x B x C in size is used for metals)

4) How many specimens does the participant typically test to determine the compression strength of a material?

5) How does the participant determine if a test is considered valid or not?

PLEASE PROVIDE ALL INFORMATION BY **1 APRIL 2018.**

If you are unable to meet this deadline please contact me.

Appendix B. Images of the Participants' Split-Hopkinson Pressure Bar (SHPB) Setups

This appendix contains images of the SHPB setups for Participants 1, 2, 4, and 5; Participant 3 did not provide an image.

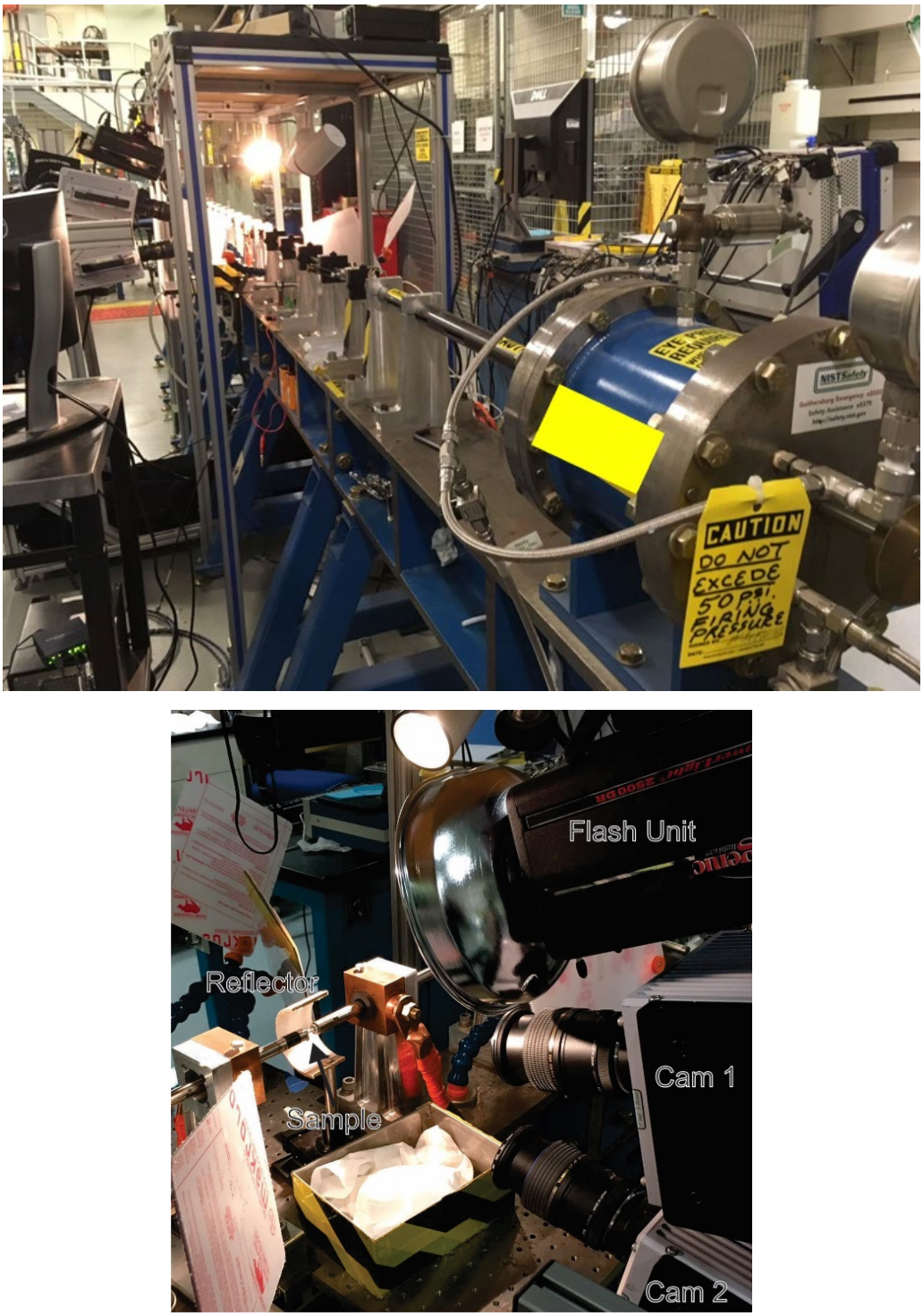

Fig. B-1 Participant 1: (top) entire test setup; (bottom) close-up of the imaging system

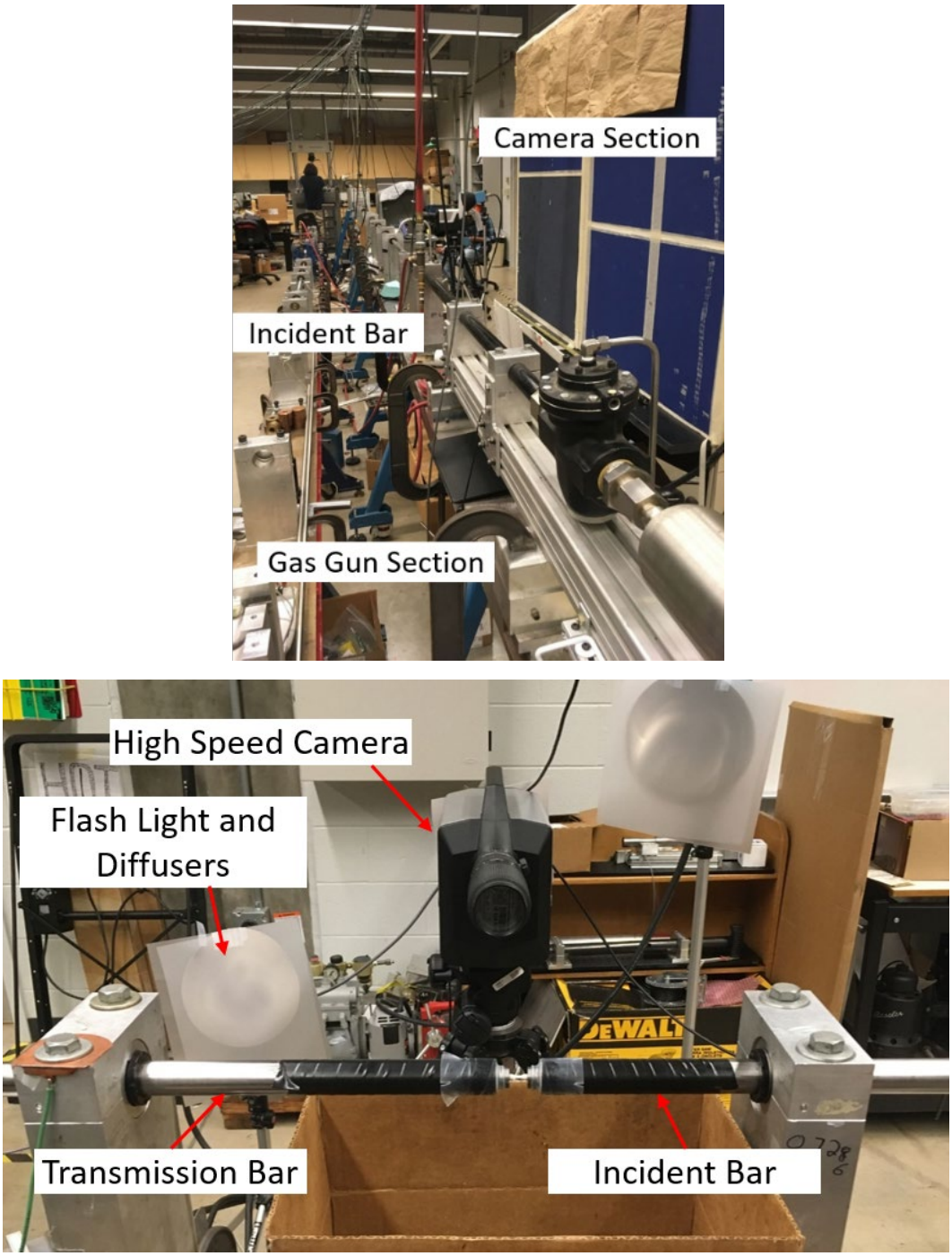

Fig. B-2 Participant 2: (top) entire SHPB setup; (bottom) close-up of specimen area with the high-speed imaging system

Fig. B-3 Participant 4: entire SHPB setup

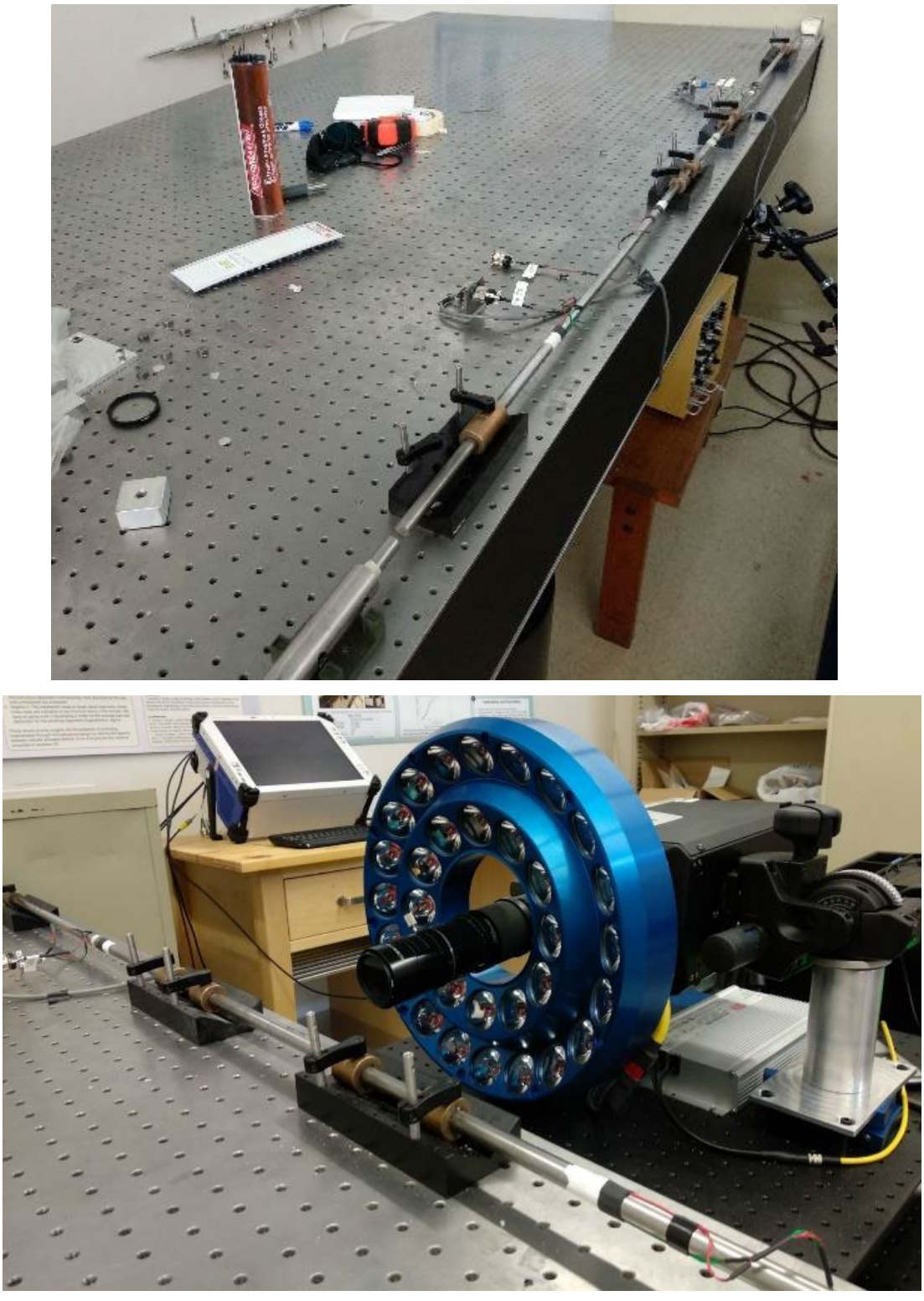

Fig. B-4 Participant 5: (top) Gas gun and striker bar are at the bottom of the image, and v-blocks house the bearings that locate and maintain the alignment of the bars; (bottom) high-speed camera with the ring light setup

Appendix C. Individual Test Results

Table C-1 Results from participant 1

Sample no.	Test no.	Ambient temp (°C)	Ambient relative humidity (%)	Strain rate (1/s)	Fracture stress (MPa)	Fracture strain	Spherical joint	Valid?
1	4077	23	18	273	4500	0.016	Y	N[a]
2	4081	23	18	115	4110	0.014	Y	Unk
3	4085	23	18	115	3700	0.014	Y	N
4	4086	23	18	115	3530	0.013	Y	N
5	4087	23	18	122	3790	0.014	Y	N
6	4088	23	18	126	4460	0.013	N	Y
7	4090	24	32	111	4040	0.013	Y	N
8	4091	24	32	112	4550	0.013	N	Y
9	4092	24	32	109	4250	0.013	N	Y
10	4093	24	32	113	4610	0.013	N	Y

[a] No rotation was noticed in the video, but the force equilibrium was poor, so the test was considered invalid.

Table C-2 Results from participant 2

Specimen NO	Nominal Length (mm)	Sample Section Diameter (mm)	Gas Gun Pressure (Psi)	Pulse Shaper Material	Pulse Shaper Diameter (mm)	Pulse Shaper Length (mm)	Temperature when tested (°F)	Humidity (%)	Is stress valid?	Is strain rate constant?	Strain rate at sample section (/s)	Compressive Strength (MPa)
s20	13.19	2.1	22	Annealed 110 Copper	6.35	2.3	71	49	Y	N	~100	5042.4
S19	13.19	2.11	27			1.5			N	N	~135	-
S18	13.19	2.1	30						N	Y	~122	-
S17	13.19	2.12	30						Y	Y	110	4644.2
S16	13.2	2.12	30						Y	Y	97	4726.0
s15	13.19	2.09	30						Y	Y	104	4967.0
s14	13.19	2.11	30						Y	Y	112	5185.9
s13	13.19	2.12	30						Y	Y	112	5029.9
s12	13.19	2.12	30						Y	Y	110	5044.7
s11	13.19	2.12	30						Y	Y	111	4699.4

Results from participant 3:

Sample 21: no strain gage on sample, no WC insert, invalid
Sample 22: no gage on sample, no WC insert, invalid
Sample 23: gage on sample, valid, 3.81 GPa
Sample 24: gage on sample, valid, 4.10 GPa
Sample 25: gage on sample, valid, 4.41 GPa
Sample 26: gage on sample, valid, 4.94 GPa
Sample 27: gage on sample, valid, 4.80 GPa
Sample 28: no gage on sample, valid, 3.81 GPa
Sample 29: gage on sample, invalid, 4.91 GPa
Sample 30: gage on sample, valid, 4.93 GPa

Average = 4.40 GPa, sample SD = 0.50 GPa

Table C-3 Results from participant 4

Specimen	Gage diameter (mm)	Specimen length (mm)	Comp. strength (GPa)	Valid?	Strain rate from bars (s^{-1})	Strain rate from DIC (s^{-1})
RR-41	2.13	13.180	4.5	Yes	120	N/A
RR-42	2.11	13.194	4.3	Yes	130	N/A
RR-43	2.12	13.196	4.4	Yes	130	N/A
RR-44	2.12	13.198	4.3	Yes	175	190
RR-45	2.13	13.210	X	X	X	X
RR-46	2.12	13.190	4.6	X	175	X
RR-47	2.12	13.198	4.7	Yes	140	190
RR-48	2.13	13.202	2.5	No	180	135
RR-49	2.12	13.207	2.4	No	190	160
RR-50	2.11	13.198	4.3	Yes	180	120

Notes: #45 the trigger had been disconnected, so no video or oscilloscope data were recorded.

#46 the oscilloscope triggered, but the camera did not, so no video files, but stress-strain data was captured; I believe it is valid based on strength value.

Table C-4 Results from participant 5

Specimen	Specimen dimensions			Pressure (psi)	Exposure (ns)	Strength (GPa)	Strain rate	Stiffness (GPa)	Failure strain (%)	Test validity
	Total length (mm)	Gauge diameter (mm)	Dumbbell diameter (mm)							
1	13.170	2.11	4.211	40	400	4.668	97.4	385	1.20	Valid
2	13.182	2.10	4.199	40	400	4.752	105.7	358	1.31	Invalid
3	13.188	2.17	4.207	40	500	4.987	97.1	359	1.39	Valid
4	13.18	2.09	4.197	40	500	5.079	137.7	391	1.24	Valid
5	13.183	2.10	4.216	40	500	4.477	83.5	416	1.06	Invalid
6	13.204	2.08	4.206	40	500	4.779	88.1	382	1.27	Valid
7	13.211	2.10	4.211	40	400	4.282	96.3	395	1.038	Invalid
8[a]	13.181	2.10	4.192	N/A	400	N/A	N/A	N/A	N/A	Invalid
9	13.192	2.09	4.209	40	400	4.096	88.0	372	1.13	Invalid
10	13.197	2.10	4.196	40	500	4.702	106.4	358	1.304	Valid

[a] There was a misfiring for test #08, so no strength or elastic properties are recorded for that test. The gas gun was accidentally triggered at an unknown pressure less than 20 psi, and the specimen likely failed on the unload.

List of Symbols, Abbreviations, and Acronyms

3D	three dimensional
COV	coefficient of variation
D	diameter
DIC	digital image correlation
FEA	finite element analysis
L	length
SHPB	split-Hopkinson pressure bar
WC	tungsten carbide

1 (PDF) DEFENSE TECHNICAL INFORMATION CTR DTIC OCA

1 (PDF) CCDC ARL FCDD RLD CL TECH LIB

19 (PDF) CCDC ARL FCDD RLW B L VARGAS A TONGE R BECKER C HOPPEL FCDD RLW M B LOVE FCDD RLW MB J PITTARI G GAZONAS D O'BRIEN FCDD RLW ME J SWAB J LASALVIA S SILTON FCDD RLW PB S SATAPATHY T WEERASOORIYA FCDD RLW PC C MEREDITH J CLAYTON D CASEM C WILLIAMS J LLOYD R LEAVY

2 (PDF) CCDC ARO FCDD RLR E D STEPP FCDD RLR EM M BAKAS